1984

The electronic structure and thermodynamics of scandium monosulfide

Jan Fujie Nakahara
Iowa State University

Nakahara, Jan Fujie

THE ELECTRONIC STRUCTURE AND THERMODYNAMICS OF SCANDIUM MONOSULFIDE

Iowa State University PH.D. 1984

The electronic structure and thermodynamics of scandium monosulfide

by

Jan Fujie Nakahara

A Dissertation Submitted to the
Graduate Faculty in Partial Fulfillment of the
Requirements for the Degree of
DOCTOR OF PHILOSOPHY

Department: Chemistry
Major: Physical Chemistry

Approved:

Signature was redacted for privacy.

In Charge of Major Work

Signature was redacted for privacy.

For the Major Department

Signature was redacted for privacy.

For the Graduate College

Iowa State University
Ames, Iowa

1984

TABLE OF CONTENTS

GENERAL INTRODUCTION

The early transition metal compounds crystallizing in the NaCl-type structure have high melting points, low vaporization rates at elevated temperatures and exhibit nonstoichiometry over a wide compositional range. The electrical transport properties range from semiconductors to metallic conductors and even to low temperature superconductors. In terms of technological applications, these compounds could be suitable high temperature coatings, conductors or heterogeneous catalysts.

The occurrence of nonstoichiometry, i.e., the formation and stability of vacancies in one or both sublattices, and long-range vacancy ordering at lower temperatures have been of research interest to experimentalists and theorists. A small amount of vacancies (a fraction of a percent at room temperature) is usually stabilized by entropic effects.[1] However, there are many compounds that cannot be categorized as such and vacancy stabilization could operate through a different mechanism. Examples of highly defective compounds are TiO (15% of the metal and nonmetal sites are unoccupied), NbO (25% of the metal and nonmetal sites are unoccupied), TiN_{1-x} (up to 40% of the nonmetal sites are unoccupied), VN_{1-x} (up to 23% of the metal sites are unoccupied) and $Sc_{1-x}S$ (up to 20% of the metal sites are unoccupied).[2]

Many of these compounds have been investigated from the perspectives of defect structure, by the usual diffraction techniques[3-9], and thermodynamic stability by high temperature vaporization experiments.[10] The mechanism for vacancy stabilization and ordering in highly defective compounds has been examined theoretically in terms of Madelung energies

for $Sc_{1-x}S$[11] and band structure[12-14] calculations. Merrick[11] concluded that vacancy ordering in $Sc_{1-x}S$ was not associated with Madelung energies (i.e., electrostatic interactions) since several alternate orderings would have lower Madelung energies and lower free energies. Huisman and coworkers,[12] reported that vacancy stabilization in TiO could be energetically driven since creation of new defect states lowered the Fermi level. Denker[13] proposed that the vacancies on both sublattices of TiO are stabilized because the creation of vacancies reduces the number of valence electrons, lowering the Fermi level and depopulating the antibonding levels. This explanation is not convincing because it assumes that the density of states is not affected by the presence of vacancies and, furthermore, suggests that vacancies should stabilize all compounds. Goodenough,[14] on the other hand, proposed that the creation of vacancies causes the cubic lattice constant to decrease, broadening the d-band due to an increase in the overlap of metal d-type wavefunctions and lowering the Fermi level. Despite these proposals for vacancy stabilization, all of which lower the Fermi level, no satisfactory theory for vacancy formation and ordering has been proposed for the nonstoichiometric early transition metal sulfides.

The scandium-sulfur system is illustrative of the early transition metal sulfides. An early study of the phases and structures of the scandium-sulfur system by Dismukes and White[8] indicated a line compound (a compound with no or very small homogeneity range), orthorhombic Sc_2S_3, and a wide rhombohedral-cubic homogeneity range between $Sc_{0.685}S$ and ScS. The powder pattern of $Sc_{0.685}S$ was indexed on the basis of a

rhombohedral unit cell with a_r = 6.33 Å and α = 33°34'. In 1974, Brozek and coworkers,[15] reported the same lattice parameters for a compound richer in scandium, $Sc_{0.75}S$. Recently, Takeshita et al.,[16] reinvestigated the composition range from ScS to Sc_2S_3 with respect to phases, electrical resistivity and thermoelectric power. X-ray powder diffraction studies and metallographic analyses provided evidence that the compounds form over two homogeneity ranges. In the first, the crystal structure varies from cubic to rhombohedral depending on temperature, in the composition range between $Sc_{1.00}S$ and $Sc_{0.75}S$. For any compound in this homogeneity range, the metal atom vacancies are ordered at low temperature corresponding to the rhombohedral structure and are disordered at high temperature corresponding to the cubic structure. The second homogeneity range is narrow in comparison to the first and is bounded between $Sc_{0.685}S$ and Sc_2S_3. An orthorhombic structure is observed in which the metal atom vacancies are partially or completely ordered.

The one-to-one monosulfide vaporizes incongruently when annealed in vacuum above 1300°C, preferentially losing the metal component to form a nonstoichiometric compound until about 20% of the metal atom sites are vacant.[9] The resulting composition is $Sc_{0.8065}S$ and vaporizes congruently, i.e., the composition of the condensed and gaseous phases are the same. At this composition, the scandium vacancies are randomly distributed in the metal sublattice at temperatures above 700°C. At 700°C the onset of a second-order phase transition, satisfying the Landau conditions, occurs in which the vacancies are confined to alternate metal

atom planes along the cubic [111] direction but randomly distributed within the plane, forming a new rhombohedral structure whose corresponding space group is a subgroup of the high temperature phase.[9,11] Franzen and coworkers,[17] observed by electron diffraction that further ordering within the partially occupied metal atom planes occurs at about 300°C. This ordering, in which the vacancies are located in almost every third rhombohedral $(1\bar{1}0)$ plane was found to be incommensurate with the metal sublattice and could be explained in terms of a population or mass density wave.

The electrical transport properties vary as a function of metal content, ranging from a semiconductor at the sulfur-rich end to a metallic conductor at the metal-rich end.[8,16] One-to-one scandium sulfide also exhibits superconductivity with a critical temperature of ~4.3 K[18] and it was observed by Moodenbaugh that as metal vacancies are introduced, superconductivity is lost. The properties of the scandium-sulfur system are summarized in Table 1.

As suggested earlier no satisfactory explanation for the defect stabilization in $Sc_{0.8065}S(s)$ has been obtained. Therefore, it is the intent of this study to determine the electronic structure of defect ScS to test the proposed energetic stabilization mechanisms of Huisman and coworkers, Denker and Goodenough. By performing the electronic structure calculations on one-to-one and an ordered defect ScS, the effects of metal atom vacancies on the electronic structure and the changes in chemical bonding induced by the vacancies can be determined. The

Table 1. Structures and properties of the scandium-sulfur system

Composition	Color	Structure	Properties	References
Sc_2S_3	yellow	orthorhombic metal vacancies ordered	n-type semiconductor ~2 eV bandgap	8
$Sc_{0.685}S$	black	orthorhombic metal vacancies partially ordered	$\rho_{300\ K} \cong 8\times10^{-3}$ Ω-cm	16
$Sc_{0.75}S$	blue	low T rhombohedral high T cubic	$\rho_{300\ K} \cong 5.5\times10^{-4}$ Ω-cm	15,16
$Sc_{0.8065}S$	purple	<700°C rhombohedral >700°C cubic ~300°C incommensurate monoclinic	vaporizes congruently second-order order-disorder transition	9,11,17
$Sc_{1.00}S$	gold	cubic	$\rho_{300\ K} \cong 4\times10^{-5}$ Ω-cm $T_c \cong 4.3$ K	8,16,18

thermodynamic stability of $Sc_{0.8065}S(s)$ will also be examined by high temperature mass loss Knudsen effusion vaporization experiments.

Explanation of Dissertation Format

The first section of the dissertation describes the electronic band structure calculations of stoichiometric ScS and a model ordered defect scandium monosulfide. The effects of metal atom vacancies on the electronic structure of ScS will be discussed. The second section describes the high temperature thermodynamics of vacancy formation in ScS. Finally, the theoretical and experimental results are summarized in an attempt to explain the defect stabilization in $Sc_{0.8065}S(s)$.

SECTION I. ELECTRONIC STRUCTURES OF STOICHIOMETRIC ScS AND ORDERED DEFECT Sc_3S_4

INTRODUCTION

There has been extensive interest in the electronic structures of the refractory transition metal compounds because of the unusual combination of properties like high melting temperature, low volatility and nonstoichiometry over a wide composition range. In the past few decades, numerous electronic structure calculations on the stoichiometric transition metal sulfides,[1-4] carbides,[5-8] nitrides[5,6,8] and oxides[5,8,9] were performed employing various theoretical techniques (e.g., APW, KKR and semiempirical LCAO-MO clusters). The common features are low lying states of nonmetal p character (p-band or valence band) with an admixture of metal d character and a complex manifold of states with metal d character (d-band or conduction band), which are separated by an energy gap in the oxides or a small amount of overlap in the remaining compounds. The strong hybridization of nonmetal p and metal d states in the valence band region is considered to be responsible for the high melting temperature and low volatility of these materials. In addition, the partial occupancy of the metal d-band is responsible for the metallic nature, hence the name conduction band.

The tendency for these compounds to form nonstoichiometrically over an extended composition range is a remarkable property. The introduction of vacancies alters the physical properties of the compound and a deeper understanding of the electronic structure of the nonstoichiometric compound is essential. Over the past five years, experimental and theoretical studies on the nonstoichiometric carbides,[7,10-14] nitrides[10,14-17] and oxides[9-11] with vacancies on the nonmetal sublattice or both

sublattices have been reported. In general, the results presented for the same class of compounds (e.g., TiC_{1-x}, TiN_{1-x}) are contradictory. Different theoretical model calculations (e.g., CPA, MS-Xα cluster calculations, APW) and different sample preparation and cleaning techniques (e.g., CVD, hot pressing) give rise to either of two results. These are: (a) the formation of new localized "defect states" between the nonmetal p-band and the Fermi level, lowering the Fermi energy and stabilizing the defect compound[9,11,14,16,17] or (b) an increase in the density of states near the Fermi level together with an upward shift in E_f, since the removal of nonmetal atoms reduces the number of p states available in the valence band region and forces the metal d electrons to occupy empty d states above the original Fermi level.[7,10,12,13,15]

Despite numerous investigations on nonstoichiometric compounds, rigorous calculations for metal-deficient transition metal sulfides have not been performed. Scandium sulfides with the compositions of $Sc_{1.00}S$ and Sc_3S_4 are prime candidates, since by performing rigorous quantum mechanical calculations, the effects of metal atom vacancies on the electronic structure and the nature of chemical bonding interactions can be elucidated.

One-to-one ScS crystallizes in the rock-salt structure with both scandium and sulfur atoms possessing nearest neighbor octahedral coordination. The composition of the model ordered defect ScS is Sc_3S_4 with 25% of the metal atom sites vacant. The unit cell which is derived from the nonprimitive rock-salt cell with the body center scandium atom removed is simple cubic as shown in Figure 1.1. The unit cell contains 3

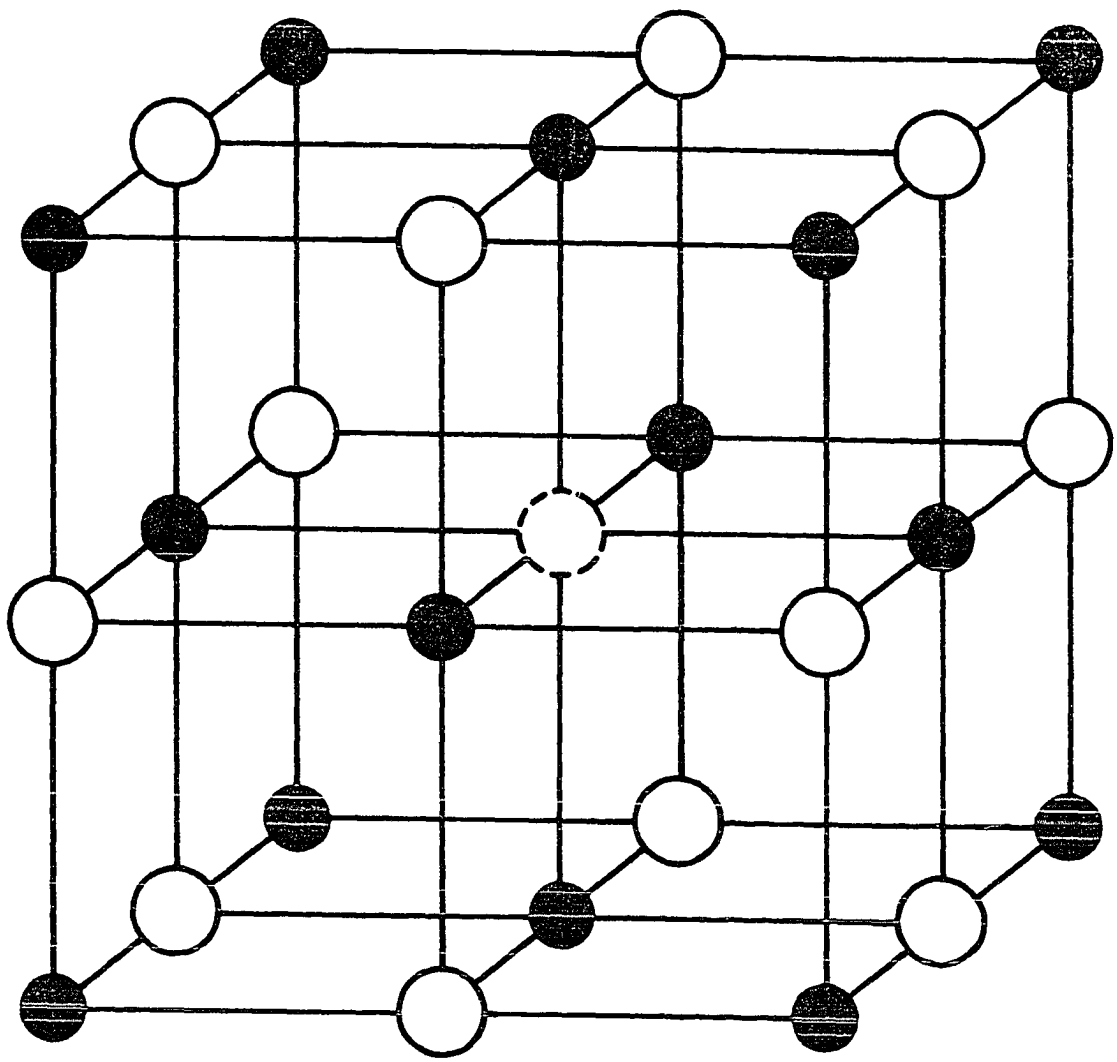

Figure 1.1. Sc_3S_4 unit cell. Black circles denote the positions of sulfur atoms; white circles denote the positions of scandium atoms; and dashed circle denotes the position of a defect

scandium atoms at (a/2,0,0), (0,a/2,0), (0,0,a/2), 4 sulfur atoms at (a/2,a/2,0), (0,a/2,a/2), (a/2,0,a/2), (0,0,0) and a scandium vacancy at (a/2,a/2,a/2). This model defect structure differs from the experimental defect compound $Sc_{0.8065}S$ with respect to composition and vacancy ordering (the (111) metal atom planes are now all partially occupied). The electronic structure of the high temperature phase of $S_{0.8065}S$ cannot be determined because the metal vacancies are randomly distributed. The unit cell of the low temperature rhombohedral form of $Sc_{0.8065}S$ would contain too many atoms, requiring an enormous amount of computer time. Despite the composition and ordering discrepancies, the results of the calculations are satisfactory, since short-range clustering of vacancies would cause only small perturbations. There are two different sulfur sites (Figure 1.1): (a) the sulfur atoms on the cube faces are surrounded by 4 scandium atoms in the plane and 2 vacant scandium sites above and below the plane, forming a square planar coordination geometry, and (b) the sulfur atoms on the cube corners remain in octahedral coordination geometry.

The effects of vacancies on the electronic structure of scandium monosulfide will be determined by comparing:

a) the energy bands (a plot of momentum vector $\vec{k}$ vs eigenvalues),

b) the total density of states (the number of electron states in the energy range E to E + dE),

c) the orbital or angular momentum decomposed densities of states to determine the origin of the peaks in the total density of states,

d) charge transfer to determine the extent of ionic character in these compounds, and

e) the charge density distributions to determine the nature of the bonding interactions.

The results of the calculations can then be compared to existing experimental results, XPS core level binding energies, specific heat and the optical spectrum, in order to verify the integrity of the theoretical model calculations.

THEORY AND METHOD

KKR Green's Function Band Structure Calculations

The electronic structures of one-to-one and ordered defect scandium monosulfide were calculated self-consistently using the nonrelativistic Korringa-Kohn-Rostoker (KKR) Green's function technique.[18] In order to gain an understanding of the distribution of electron states in solids, solutions to the Schrödinger equation are sought. In atomic units, the Schrödinger equation is written as

$$(-\nabla^2 + V(\vec{r}) - E)\,\Psi\,(\vec{r}) = 0, \qquad (1.1)$$

where $V(\vec{r})$ is the crystal potential which has the periodicity of the lattice. To simplify the task of solving the fundamental equation, the true crystal potential is replaced by a muffin tin potential. In the muffin tin potential approximation, a sphere is centered on each atomic position in the unit cell such that they do not overlap and inside the sphere the potential is spherically averaged. In the region between the spheres, the interstitial region, a volume averaged potential is substituted.

The muffin tin potential was generated by first calculating the Hartree-Fock-Slater self-consistent atomic charge densities. Secondly, following the procedure described by Mattheiss,[19] the atomic charge densities were superposed to yield the spherically averaged atomic potentials. The atomic and crystal potentials also consisted of an exchange-correlation component using the Hedin-Lundqvist approximation.[20]

Within each muffin tin sphere, the wavefunction is composed of a finite sum of spherical harmonics multiplied by the radial function, which is dependent only on the azimuthal quantum number due to the spherically symmetric nature of the crystal potential. That is,

$$\psi(\vec{r}) = \sum_{\ell=0}^{\ell} \sum_{m=-\ell}^{\ell} C_{\ell,m}(E)\, R_{\ell,E}(r)\, Y_{\ell,m}(\hat{r}), \tag{1.2}$$

where ℓ and m represent the angular momentum component, $C_{\ell,m}(E)$ is an expansion coefficient determined by solving a set of linear equations, $R_{\ell,E}(r)$'s are solutions to the radial Schrödinger equation for energy E and $Y_{\ell,m}(\hat{r})$'s are the spherical harmonics. For both ScS and Sc_3S_4, the expansion included spherical harmonics through $\ell = 2$ within the Sc and S spheres, but only through $\ell = 1$ within the Sc vacancy sphere.

The Green's function, $G(\vec{r},\vec{r}')$, is defined by the differential equation

$$(-\nabla^2 - E)\, G(\vec{r},\vec{r}') = -\delta(\vec{r}-\vec{r}'). \tag{1.3}$$

Now if the Green's function is applied to the Schrödinger equation,

$$(-\nabla^2 - E)\, \Psi(\vec{r}) = -V(\vec{r})\, \Psi(\vec{r}), \tag{1.4}$$

the resulting electron wavefunction is an integral equation,

$$\Psi(\vec{r}) = \int_{\substack{\text{cell}\\ \text{volume}}} G(\vec{r},\vec{r}')\, V(\vec{r}')\, \Psi(\vec{r}')\, d^3r'. \tag{1.5}$$

The integral over the cell volume can be replaced by the integral over just the muffin tin spheres because of the muffin tin potential approximation. Furthermore, the volume integral can be rewritten as a surface

integral by making use of Schrödinger's equation and the definition of Green's function. That is,

$$0 = \Psi(\vec{r}) - \int_{\substack{\text{muffin tin}\\ \text{volume}}} G(\vec{r},\vec{r}')\, V(\vec{r}')\, \Psi(\vec{r}')\, d^3r' \qquad (1.6a)$$

$$= \Psi(\vec{r}) - \int_{\substack{\text{muffin tin}\\ \text{volume}}} G(\vec{r},\vec{r}')\, (\nabla'^2 + E)\, \Psi(\vec{r}')\, d^3r' \qquad (1.6b)$$

$$= \int_{\substack{\text{muffin tin}\\ \text{surface}}} \left[G(\vec{r},\vec{r}')\, \frac{\partial}{\partial r'}\, \Psi(\vec{r}') - \Psi(\vec{r}')\, \frac{\partial}{\partial r'}\, G(\vec{r},\vec{r}')\right] ds'. \qquad (1.6c)$$

The final result is that once the wavefunction inside the muffin tin spheres and the form of G at the muffin tin boundaries are known, the surface integral equation (equation 1.6c) reduces to a set of homogeneous linear algebraic equations. The solutions to the set of equations are determined by finding the zeros of the secular determinant by allowing the energy to vary between a minimum and maximum value at a particular wave vector $\vec{k}$. The resulting set of energies and $\vec{k}$'s produces the dispersion relation $E = E(\vec{k})$ which is called the energy bandplot. The wavefunctions $\Psi(\vec{r})$ are then obtained by substituting $E(\vec{k})$ back into the set of linear equations.

In order to resolve the question of electron distribution and charge transfer in solids, an accurate representation of the charge density is desired and thus requires the self-consistent process. The valence electrons of the atoms comprising the unit cell create an electrostatic potential from which a charge density can be generated by solving Poisson's equation within the muffin tin spheres. This charge density

is then used in Schrödinger's equation to generate a set of wavefunctions. In turn, these wavefunctions generate a new charge density. This process is repeated until the set of wavefunctions from two consecutive iterations do not change.

The self-consistent procedure is depicted in the flow diagram (Figure 1.2). Self-consistency was achieved when the maximum error in the total charge density (core + valence) between successive iterations was less than 0.003 electrons/$(a.u.)^3$. The wavefunctions and eigenvalues were evaluated for 20 points uniformly distributed in $^1/_{48}$th of the first Brillouin zone (BZ). The remainder of the first BZ is generated when the 48 group operations are applied to the 20 points in the irreducible piece of the BZ. For one-to-one ScS, the wavefunctions and eigenvalues of 9 bands were evaluated in the irreducible wedge of the face-centered cubic BZ. On the other hand, the wavefunctions and eigenvalues of 30 bands were evaluated in the irreducible wedge of the simple cubic BZ. The lattice constant was taken to be 5.192 Å in both calculations. The radius of the Sc muffin tin sphere was 1.397 Å and 1.196 Å for the S muffin tin sphere. The empty site in the ordered defect structure had a radius of 1.397 Å. In both structures, 53% of the cell volume was occupied by muffin tin spheres.

In order to obtain the energy dispersion bandplot, additional $\vec{k}$ points were needed to sample the irreducible piece of the BZ. Therefore, for the final determination of wavefunctions and eigenvalues, 60 $\vec{k}$ points were used. The energy bands were fit to a Fourier series using 40 symmetrized plane waves with a maximum root mean square error of 2.75 mRy.

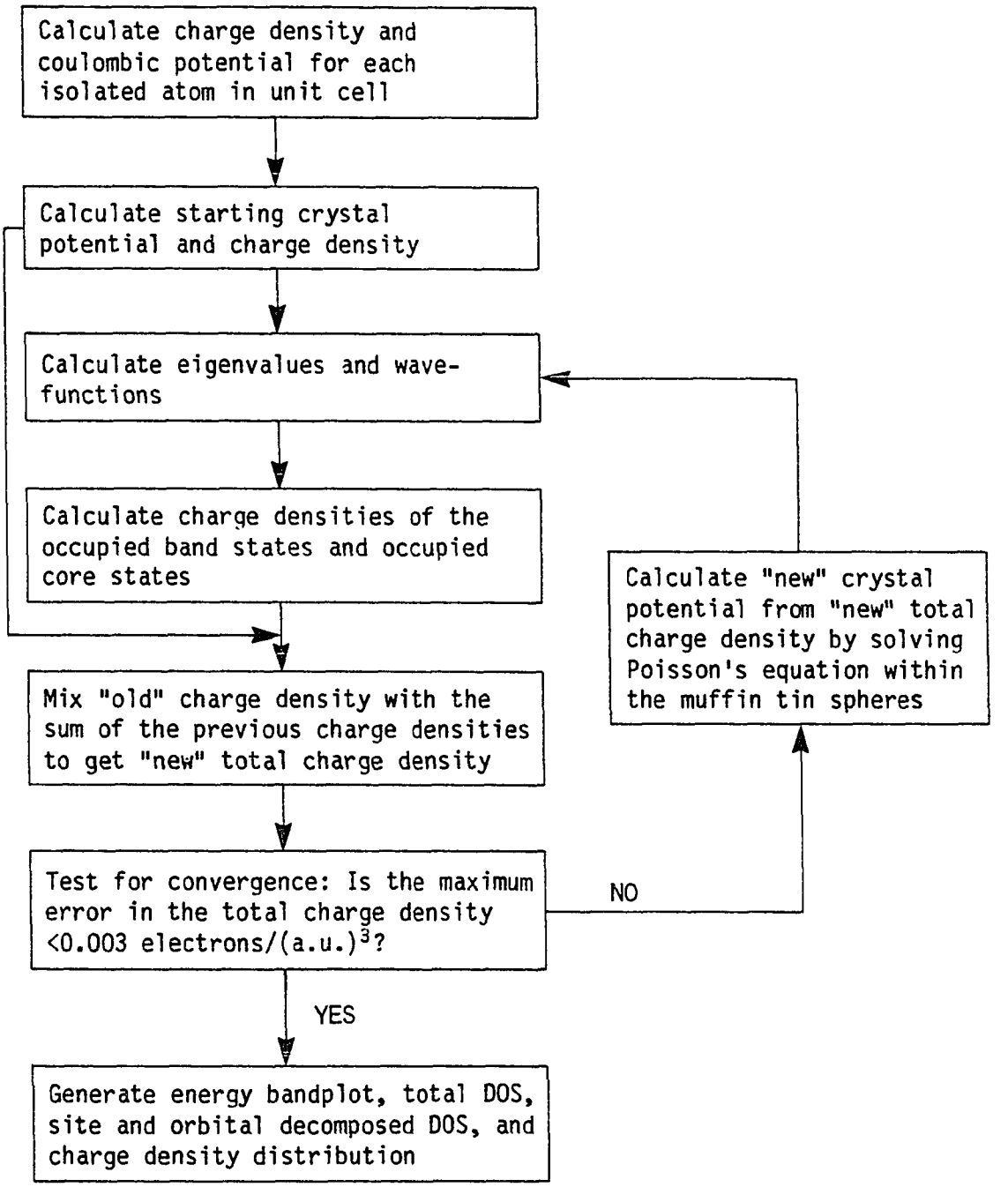

Figure 1.2. Flow diagram depicting the self-consistent process. Each box represents a separate program

The densities of states, the number of electron states in the energy range E to E + dE, were obtained by the method of Jepsen and Andersen[21] by summation over microtetrahedra into which the BZ was divided. The densities of states for the one-to-one calculation were evaluated using 2048 tetrahedra in the irreducible $^1/_{48}$th of the BZ and 512 tetrahedra for the ordered defect calculation. The factor of 4 difference is due to the fact that the fcc BZ is 4 times larger than the simple cubic BZ.

To investigate the character of bonding interactions, the charge densities for each set of bands and within each muffin tin sphere were determined by calculating the expansion,

$$\rho(\vec{r}) = \sum_{\ell,m} \rho_{\ell,m}(r)\, Y_{\ell,m}(\hat{r}), \tag{1.7}$$

where ℓ and m represent the angular momentum component and $\rho_{\ell,m}(r)$ is the charge density contribution from the (ℓ,m) component. It is required that for each muffin tin sphere, $\rho(\vec{r})$ must transform as the totally symmetric irreducible representation for all operations of the point group, O_h symmetry for the octahedral sites and D_{4h} symmetry for the square planar sites. Therefore, for each muffin tin sphere the number of (ℓ,m) components will be governed by the site symmetry. The only nonvanishing elements of $\rho_{\ell,m}(r)$ for the expansion of the charge density through $\ell = 4$ are $(\ell,m) = \{(0,0), (4,0), (4,4)\}$ on the octahedral Sc and S sites. For the ordered defect monosulfide, the nonvanishing elements for an atom at a square planar site are $(\ell,m) = \{(0,0), (2,0), (4,0), (4,4)\}$ for the 4-fold rotation axis along the z direction and

$(\ell,m) = \{(0,0), (2,0), (2,2), (4,0), (4,2), (4,4)\}$ for the 4-fold rotation axis along the x and y directions. The nonvanishing elements are constructed by,

$$\rho_{\ell,m}(r) = \sum_{E_{min}<E<E_{max}} \sum_{\ell_1,m_1} \sum_{\ell_2,m_2} I^{\ell,m}_{\substack{\ell_1,m_1 \\ \ell_2,m_2}} R_{\ell_1,E}(r)\, R_{\ell_2,E}(r)\, C^{*}_{\ell_1,m_1}(E)\, C_{\ell_2,m_2}(E), \tag{1.8}$$

where $I^{\ell,m}_{\substack{\ell_1,m_1 \\ \ell_2,m_2}}$ is the Gaunt coefficient given by,

$$I^{\ell,m}_{\substack{\ell_1,m_1 \\ \ell_2,m_2}} = \int Y^{*}_{\ell,m}\, Y^{*}_{\ell_1,m_1}\, Y_{\ell_2,m_2}\, d\Omega, \tag{1.9}$$

and the minimum and maximum energies are determined from the angular momentum decomposed densities of states.

RESULTS

Energy Bandplots

The eigenvalues E were plotted against the momentum vector $\vec{k}$ along the high symmetry directions of the simple cubic BZ ($\Gamma \rightarrow X \rightarrow M \rightarrow R \rightarrow \Gamma$, $X \rightarrow R$) to produce the energy bandplots. The simple cubic BZ is shown in Figure 1.3; the tetrahedron bounded by the high symmetry points represents an irreducible piece of the BZ.

Figure 1.4 shows the fcc eigenvalues of one-to-one ScS plotted in a reduced zone. Since the simple cubic BZ is one-fourth the volume of the fcc BZ, the bands for one-to-one ScS are back-folded, resulting in a larger number of bands. This is equivalent to four ScS formula units per simple cubic unit cell or Sc_4S_4 in short. Figure 1.5 shows the energy bands of ordered defect Sc_3S_4. The energies in Sc_4S_4 have been shifted by -0.043 Ry so that the bottoms of the sulfur p-bands coincide, and is equal to the difference in the muffin tin zeros of the two crystal potentials.

The common features below the Fermi level at the zone center are the four low lying Γ_{15} states composed primarily of sulfur 3p-states and a $\Gamma_{25'}$ state composed of scandium 3d-states which overlaps with the sulfur 3p-states, constituting the valence band region. Above the Fermi level, a complex band system is observed corresponding to the unoccupied Sc 3d states. The Fermi level crosses the Sc 3d bands, hereafter called the conduction bands, giving rise to the metallic conductivity of these materials. The differences at Γ are primarily the reduced degeneracies

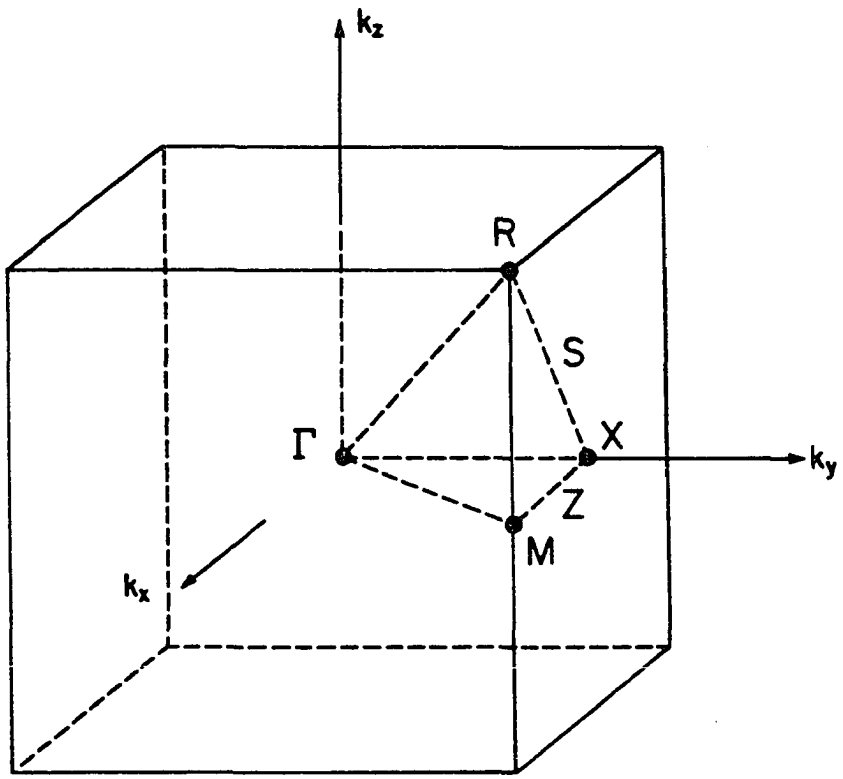

Figure 1.3. The simple cubic Brillouin zone with the high symmetry points indicated

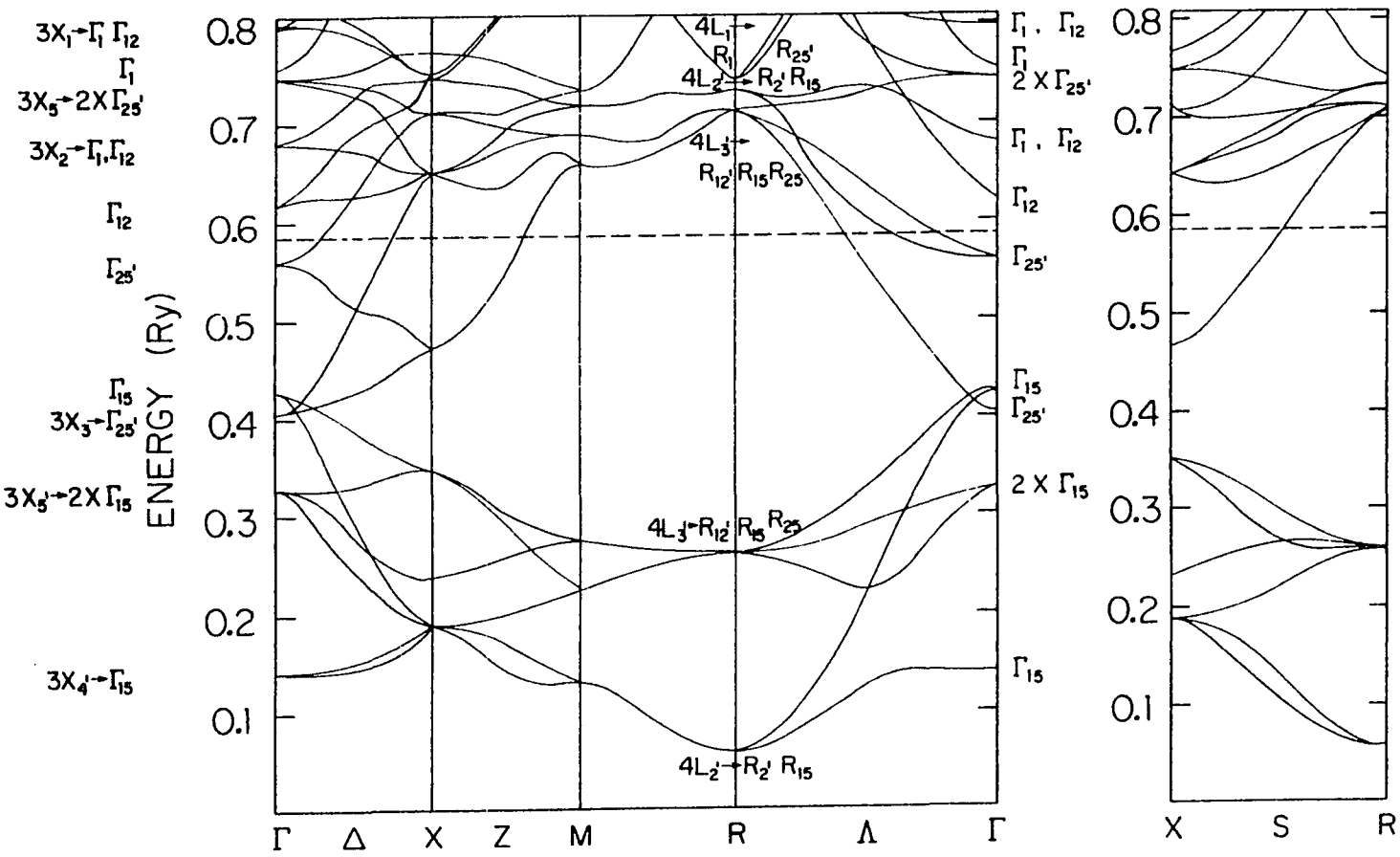

Figure 1.4. Energy bandplot for NaCl-type ScS drawn in the simple cubic BZ. States are labeled by both fcc and simple cubic representations

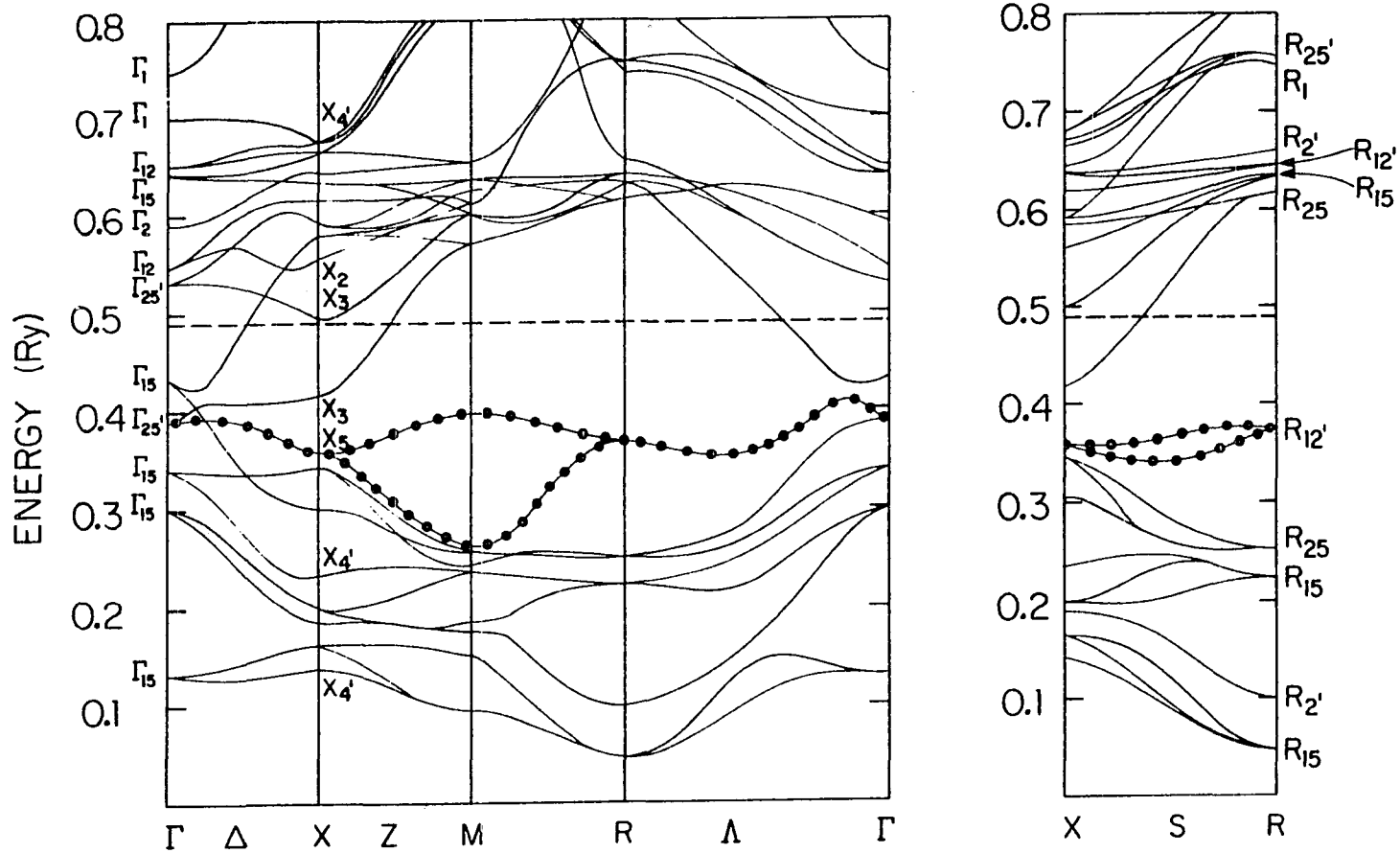

Figure 1.5. Energy bandplot for Sc_3S_4. Bands marked in solid circles are sulfur p-nonbonding states

and the absence of a $\Gamma_{25'}$ and a Γ_{12} state between 0.75 and 0.80 Ry in Sc_3S_4. The $\Gamma_{25'}$ and Γ_{12} states are presumably the nonbonding Sc d states that are present in Sc_4S_4 but absent in Sc_3S_4.

The removal of a Sc atom reduces degeneracies and generates band splittings. An example of band splitting can be seen between the high symmetry points M and R. In Sc_4S_4, the 4-fold degenerate band from 0.28 Ry at M to 0.26 Ry at R ($R_{12'}$, R_{15}, R_{25}) has been split in Sc_3S_4 into two singly degenerate bands ($R_{12'}$) and a 2-fold degenerate band (R_{25}) which are separated by a maximum of 0.12 Ry at R. A second example of band splitting is the 2-fold degenerate X_3 states in Sc_4S_4 at 0.47 Ry. These X_3 states are degenerate because the bands are plotted in a reduced zone. In Sc_3S_4, these two states are split along the Z and S directions, raising and lowering states near the Fermi level.

Throughout the BZ in Sc_3S_4, there are states marked in solid circles in a narrow energy range (0.27 - 0.41 Ry) with little dispersion and localized, which are absent in the corresponding energy range in Sc_4S_4. These are not new states since there are generally 12 bands below the fourth Γ_{15} state in both calculations, but rather these are states redistributed by the introduction of a vacancy.

Total and Orbital or Angular Momentum Decomposed Densities of States

The total density of states (DOS) for Sc_4S_4 and Sc_3S_4 (Figure 1.6) were obtained from the eigenvalues using the tetrahedron method of Jepsen and Andersen. Generally, flat regions of the energy bandplot give rise to maxima in the DOS and rapidly varying bands give rise to smaller DOS.

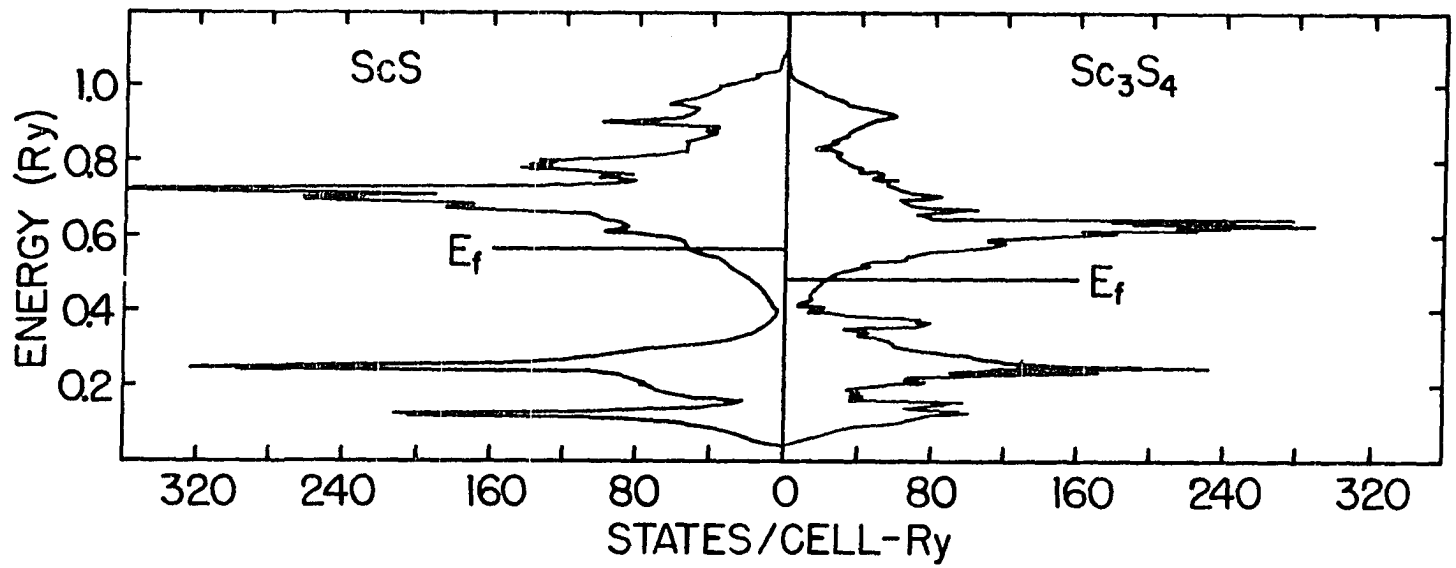

Figure 1.6. Total densities of states for Sc_4S_4 and Sc_3S_4

There are several features that are observed in the DOS for Sc_3S_4:

a) a lowering of the Fermi level from 0.57 to 0.49 Ry,

b) a shifting of the d-band maximum to lower energies,

c) a narrowing of the d-band region, and

d) a new feature in the DOS at 0.37 Ry which is narrow and localized.

The density of states at the Fermi level is decreased from 56.2 to 21.2 states/cell•Ry when vacancies are introduced into the metal sublattice. This observation is opposite to that reported for vacancies in the nonmetal sublattice.[7,10,12,13,15] The apparent decrease in the DOS at E_f is due to the reduction in number of Sc conduction electrons.

In order to illuminate the character of chemical bonding in terms of atomic orbitals, the wavefunctions were projected out onto spherical harmonics to produce the orbital or angular momentum decomposed densities of states. More importantly, the character of the new peak in the total DOS of Sc_3S_4 can be understood.

In Figures 1.7 and 1.8, the partial DOS inside the Sc muffin tin sphere with the p- and d-type wavefunction contributions are depicted. For both Sc_4S_4 and Sc_3S_4, the features are similar. At low energies between 0.04 and 0.40 Ry, the partial DOS is an admixture of Sc p and d states. Between 0.40 and 1.0 Ry the partial DOS is primarily of Sc 3d states and the partial occupancy of this band system is responsible for the metallic conductivity of these compounds.

The Sc d-type wavefunctions were further decomposed into e_g (d_{z^2}, $d_{x^2-y^2}$) and t_{2g} (d_{xy}, d_{xz}, d_{yz}) components (Figure 1.9). In both

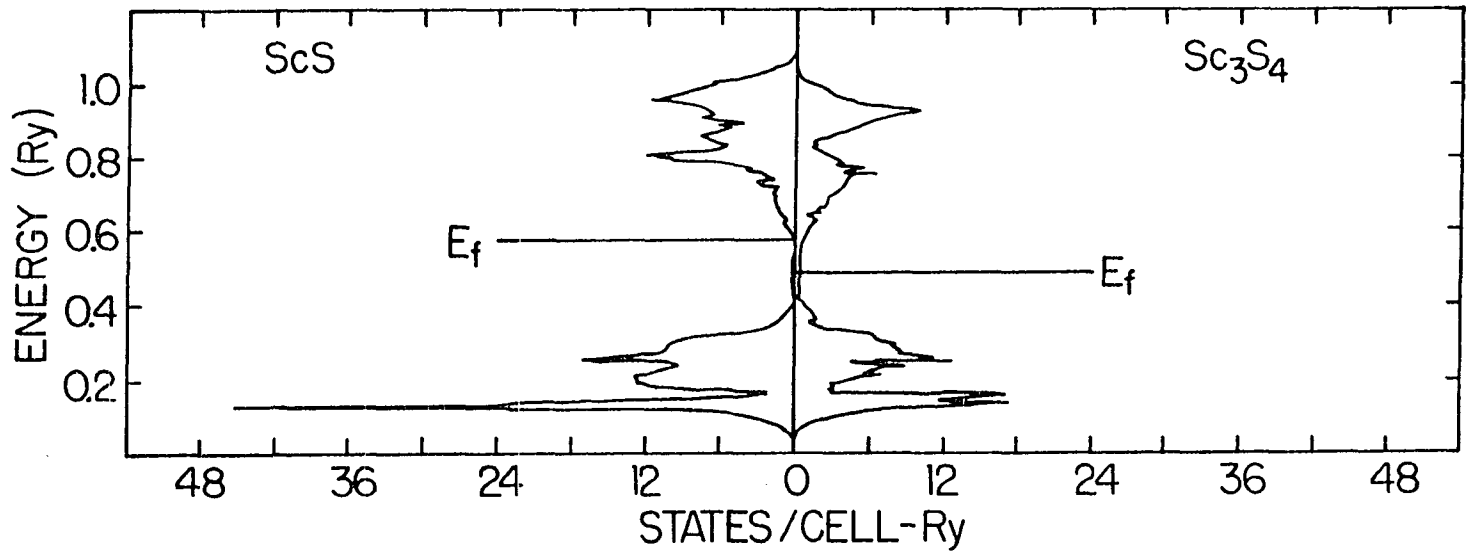

Figure 1.7. Angular momentum projected DOS for $\ell = 1$ on a scandium site

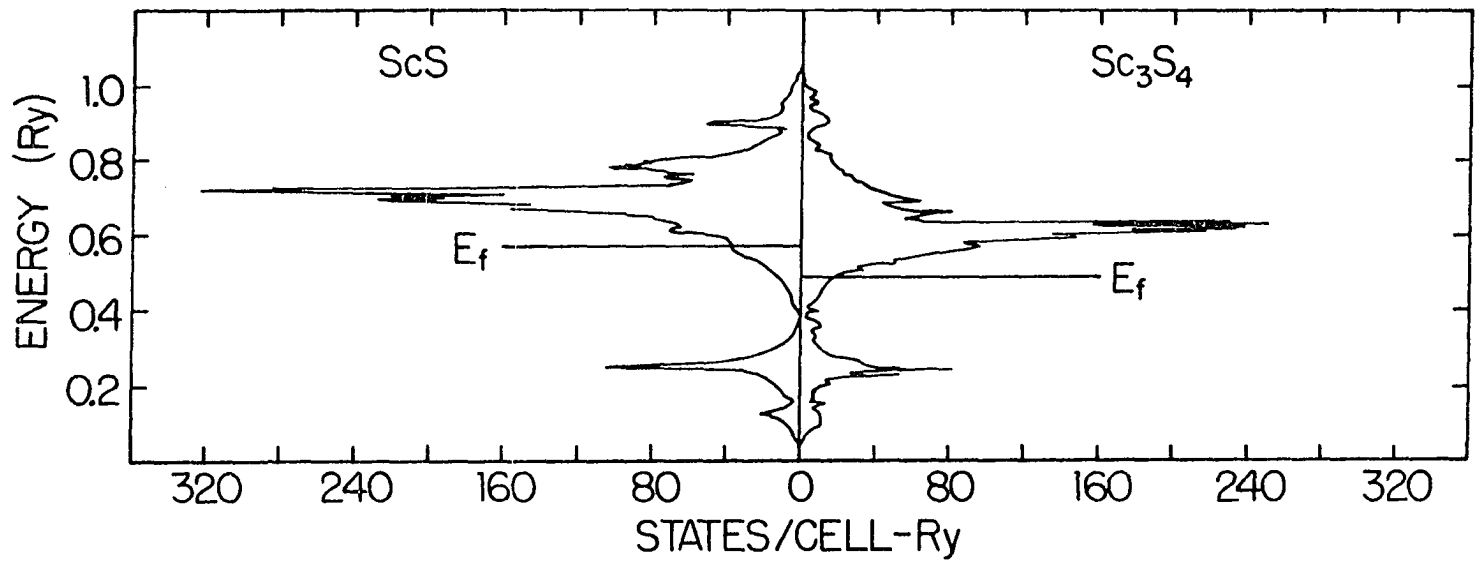

Figure 1.8. Angular momentum projected DOS for $\ell = 2$ on a scandium site

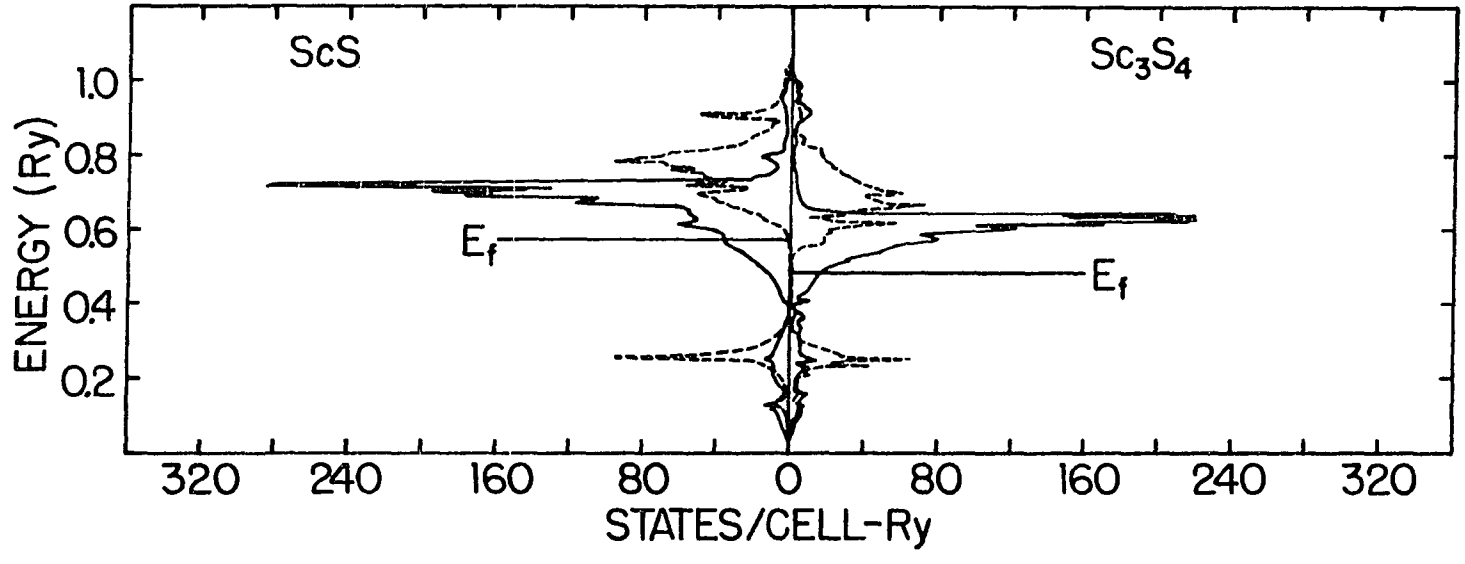

Figure 1.9. e_g (---) and t_{2g} (—) densities of states on a scandium site

Sc_4S_4 and Sc_3S_4, the low lying states are of e_g character and the states near and above the Fermi level are of t_{2g} character. This result is consistent with previous calculations on the rock-salt type transition metal sulfides.[1,2]

The $\ell = 1$ and $\ell = 2$ partial DOS inside the sulfur muffin tin spheres are shown in Figures 1.10 and 1.11. The DOS inside the nonequivalent sulfur sites in Sc_3S_4 are shown separately. For both Sc_4S_4 and Sc_3S_4, the partial DOS between 0.04 and 0.40 Ry is predominantly S 3p-like with some Sc e_g-like states. This pd hybridization is the covalent metal-nonmetal bonding interaction.

A noticeable difference is the new feature at 0.37 Ry in the square planar S partial DOS with entirely p-type character. The metal t_{2g} contribution is absent at this energy as was shown in the Sc e_g-t_{2g} angular momentum decomposition.

The position of the new peak on the high energy side of the main sulfur peak is not unreasonable. This could be explained in terms of a simple molecular orbital model. Consider a sulfur atom surrounded by 6 Sc atoms in an octahedral arrangement, with p orbitals centered on S and d orbitals on Sc. The nonmetal p orbitals will overlap with the metal e_g orbitals forming bonding and antibonding combinations, lowering the energy of this configuration. Now if 2 Sc atoms are removed from the apices of the octahedron, as in Sc_3S_4, the p_z orbital on S no longer can overlap with the d_{z^2} orbital on Sc. The result is that there will be some nonbonding p states associated with S at an energy greater

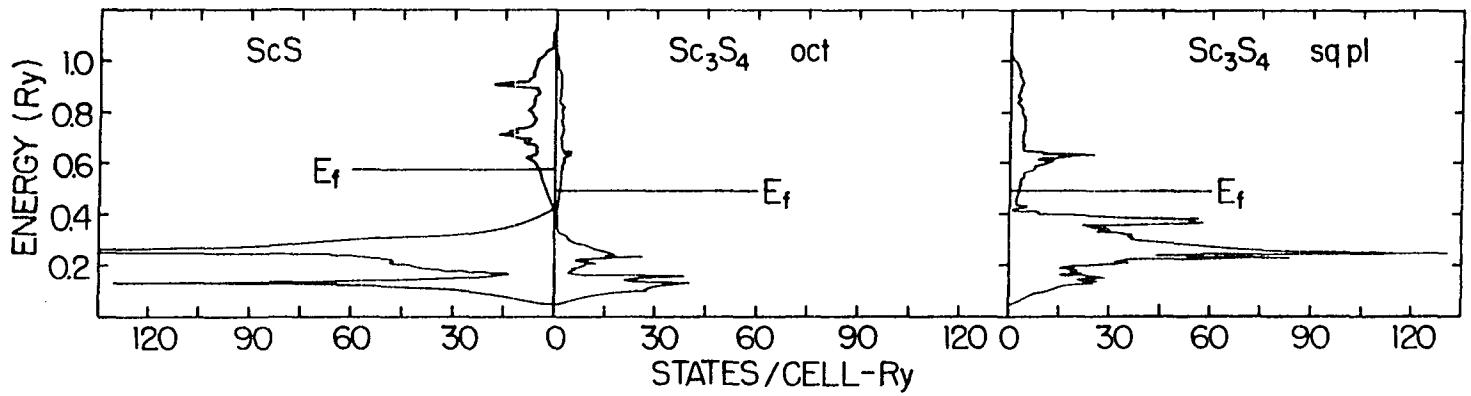

Figure 1.10. Angular momentum projected DOS for $\ell = 1$ on a sulfur site

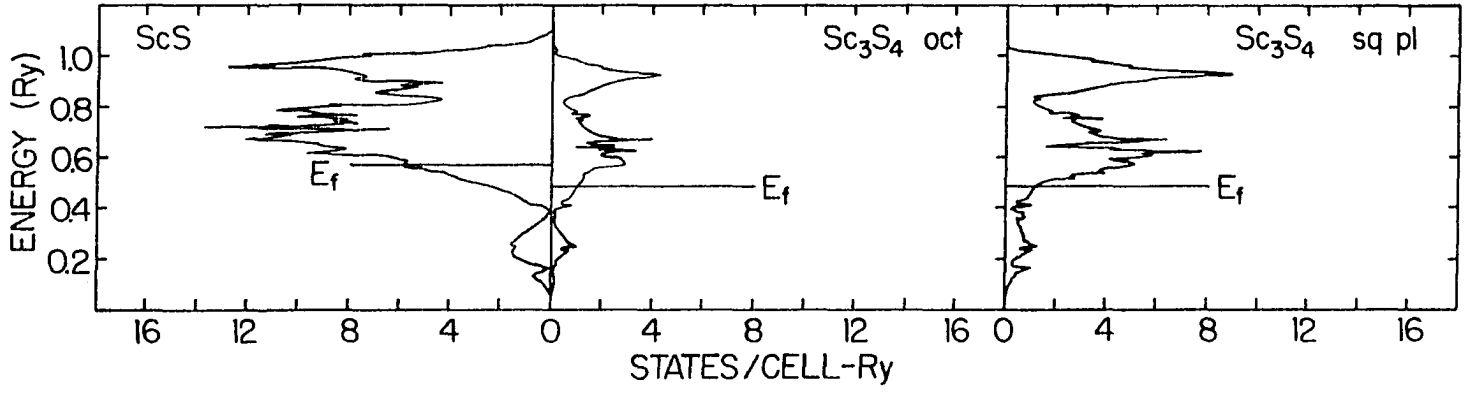

Figure 1.11. Angular momentum projected DOS for $\ell = 2$ on a sulfur site

than the energy of the bonding levels, raising the energy of the square planar combination.

In order to test the result of the molecular orbital model, the three nonequivalent p orbitals on the square planar S atoms were decomposed into projections which lie in the plane of the Sc atoms and those along the vacancy-vacancy axis. The top panel of Figure 1.12 displays the partial DOS in the plane of the scandium atoms or the bonding modes. The bottom panel shows the partial DOS of the square planar S atoms directed along the vacancy-vacancy axis or the nonbonding modes. It is clear from this decomposition that the new peak at 0.37 Ry originates entirely from the nonbonding states associated with the square planar S p orbitals directed along a vacancy-vacancy axis. This result is in agreement with that predicted by the molecular orbital model.

The contribution to the total DOS of Sc_3S_4 from the Sc vacancy was determined but the charge contribution was negligible, contrary to results obtained from calculations with defects in the nonmetal or nonmetal and metal sublattices.[9,10,14] This result suggests that electron localization at the vacancy sites is not occurring.

Charge Transfer

In order to address the question of ionic character and changing ionicity with stoichiometry, that is, is scandium in $Sc_{1-x}S$ a mixture of Sc^{2+} and Sc^{3+}, charge transfer has been determined theoretically and compared to experimental results.

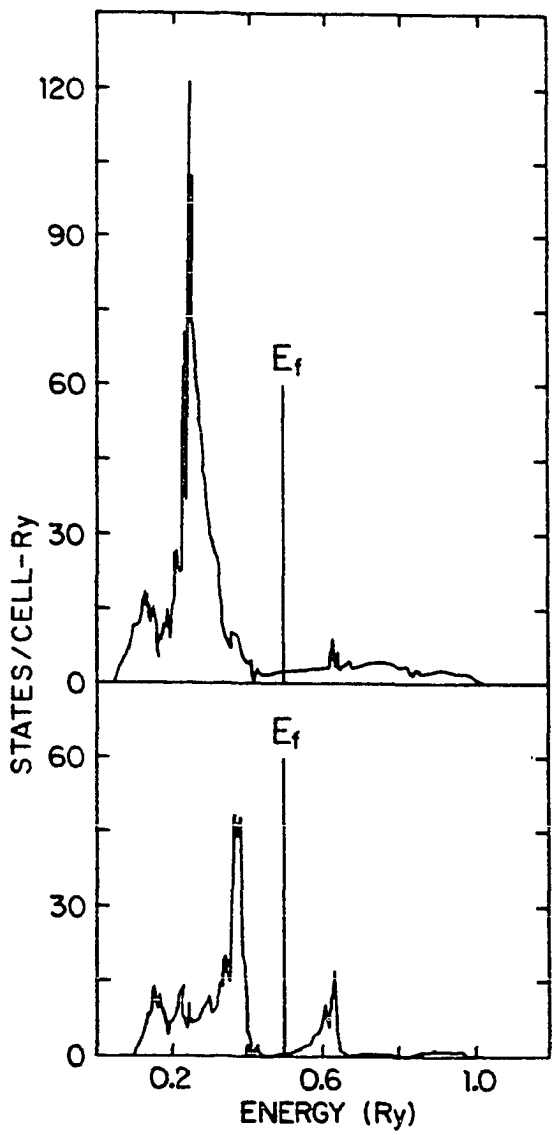

Figure 1.12. Square planar sulfur $\ell = 1$ DOS projected in the plane of Sc atoms (top) and along the vacancy-vacancy axis (bottom)

Charge transfer from metal to nonmetal in stoichiometric and non-stoichiometric transition metal carbides, nitrides and oxides has been known.[8-10,13,16] Charge transfer can be investigated by examining the core level binding energies in the compound and comparing them with those in the pure material. The core level binding energies are obtained from XPS or ESCA measurements.

Merrick[2] has reported the scandium and sulfur 2p core level binding energies for the pure elements, two scandium sulfide compounds and two ionic alkaline earth sulfides with the NaCl-type structure. The results imply a small charge transfer from Sc to S and moreover, within experimental error, there are no changes in the scandium and sulfur binding energies with increasing Sc vacancy concentration. The absence of a core level shift in Sc is evidence that two oxidation states of Sc do not coexist in the nonstoichiometric material. It was also concluded that strong covalent interactions prevailed in the scandium sulfide materials since only small binding energy shifts were measured for scandium and sulfur relative to the pure elements.

A method of determining charge transfer theoretically is to examine the difference between the self-consistent total electronic charge and the overlapping atomic charge for each type of atom in the unit cell. From Table 1.1, charge transfer from Sc to S is approximately the same in ScS and Sc_3S_4, namely a loss of about 0.3 electrons from the Sc muffin tin sphere and a gain of about 0.06 electrons in the S muffin tin sphere. These theoretical results are in complete agreement with the XPS core level binding energies, in that the valency of the scandium atoms does

Table 1.1. Theoretical total electronic charge in electrons/(a.u.)^3

		Sc	oct S	sq pl S	Sc vacancy	Interstitial
	KKR self-consistent	19.5966	14.9760			2.4274
ScS	overlapping atomic	19.8543	14.9196			2.2261
	difference	-0.2577	0.0564			0.2013
	KKR self-consistent	19.5289	15.0217	14.8158	0.3435	2.1502
Sc_3S_4	overlapping atomic	19.8127	14.9143	14.7959	0.4819	1.9445
	difference	-0.2838	0.1074	0.0199	-0.1384	0.2057

not change as a function of stoichiometry. A likely explanation for this result is an increased metal d-nonmetal p hybridization in the valence band region. (See the section on charge density analysis.)

These results, however, are not consistent with what would be expected from the simple ionic model. If this were the case, then the S atoms in Sc_3S_4 would have a -2 charge and the Sc atoms would need to yield 2 electrons, with a net charge transfer of 0.67 electrons from Sc to S. This proves that a simplistic ionic model does not apply to bonding in scandium sulfide.

Comparison to UPS Spectra

In addition to measuring the XPS spectrum, the valence-conduction band spectrum was obtained. There is a one-to-one correspondence between the observed photoelectron peaks and the peaks in the broadened total DOS below the Fermi level. The theoretical DOS were broadened with a 1 eV half-width Gaussian function to adjust for instrumental resolution.

The UPS spectra shown in the top panel of Figure 1.13 were obtained by passing $H_2S(g)$ over a thin foil of Sc metal at two different temperatures.[22] One explanation for the different spectra is that at high temperature (Figure 1.13a), the Sc and S diffusion rates are sufficiently rapid to form a near one-to-one surface stoichiometry. However, at a lower temperature (Figure 1.13b), the Sc diffusion rate decreases and the resulting surface composition is metal deficient giving rise to the additional side peak 3 eV below the Fermi level.

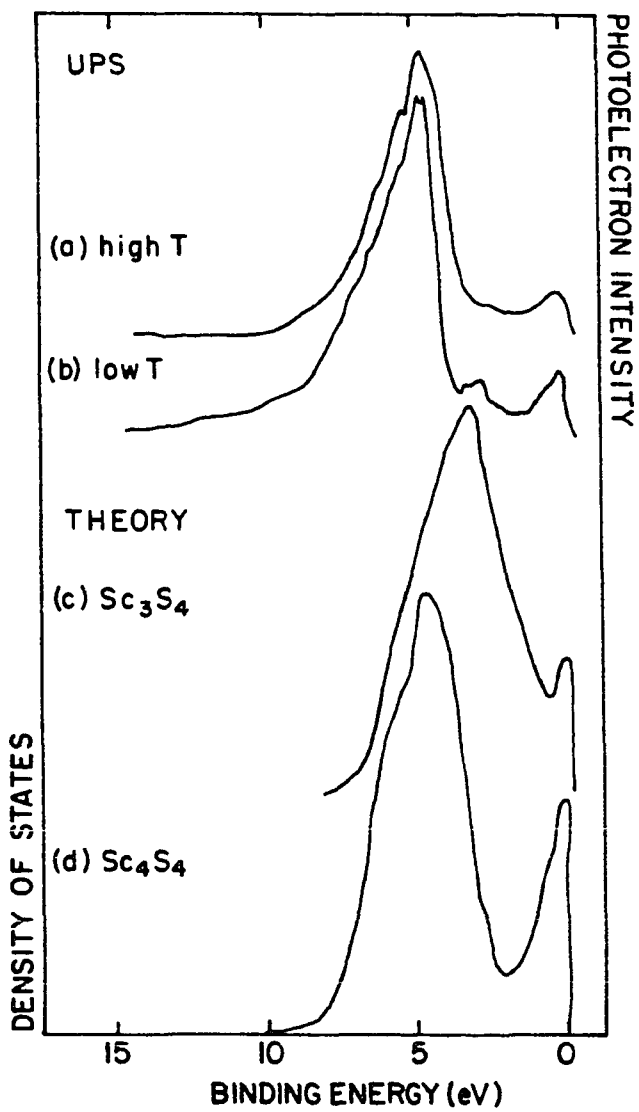

Figure 1.13. Experimental UPS spectra of scandium sulfide (a,b) and theoretical total densities of states for Sc_3S_4 (c) and Sc_4S_4 (d)

There is good agreement with respect to peak position between the high temperature UPS spectrum (Figure 1.13a) and the broadened total DOS of Sc_4S_4 (Figure 1.13d). The peak near the Fermi level originates from the occupied Sc 3d states and the peak between 4 and 9 eV originates from the S 3p states.

There is fair agreement between the low temperature UPS spectrum (Figure 1.13b) and the broadened total DOS of Sc_3S_4 (Figure 1.13c) with respect to the position of the additional peak and the maximum in the S 3p states in Sc_3S_4. The peak heights and positions in the low temperature spectrum suggest sampling of a two phase mixture or the occurrence of surface segregation, i.e., small islands of $Sc_{1-x}S$ dispersed in a stoichiometric ScS matrix.

The similarity in features between the experimental UPS spectra and the broadened theoretical total DOS provides support for the theoretical model chosen to represent the electron distribution in bulk solids.

Charge Density Analysis

Electron density contours in a plane perpendicular to the [111] direction were determined to evaluate the bonding interactions in ScS and the changes when metal vacancies are introduced. The electron distributions were separated into two distinct energy ranges, namely the p-band or valence band energy range and the d-band or conduction band energy range, as determined from the angular momentum decomposed densities of states.

The NaCl unit cell is shown in Figure 1.14 to facilitate the discussion of the electron distribution. Also shown are the sulfur atoms

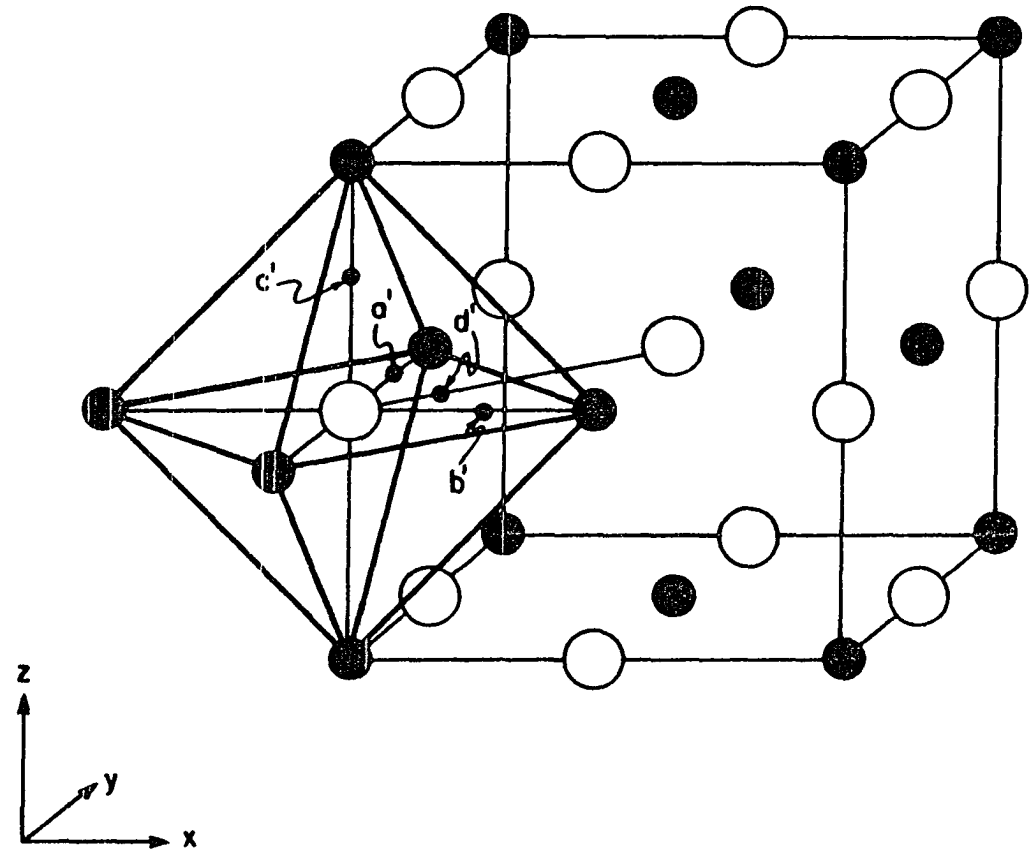

Figure 1.14. The NaCl unit cell. Large dark solid circles denote the position of the sulfur atoms; open solid circles denote the position of the metal atoms. The plot plane is perpendicular to the [111] direction. The points a', b' and c' denote the location at which the plot plane intersects the Sc-S bond axes. The point d' denotes the location at which the plot plane intersects the Sc-Sc bond axis

forming an octahedron around the scandium atom. The plot plane is perpendicular to the [111] direction and slices through three nonmetal muffin tin spheres along the x,y,z axes and a metal muffin tin sphere. The points a', b' and c' denote the location at which the plot plane intersects the metal-nonmetal bond axes. The point d' denotes the location at which the plot plane intersects the metal-metal bond axis. The plot plane also contains two other equivalent points along metal-metal bond axes which are not shown.

The charge density distribution for NaCl-type ScS in the valence band region (Figure 1.15) principally illustrates the metal e_g-nonmetal p σ-bonding interactions (0.0186 electrons/(a.u.)^3). The charge density within the sulfur muffin tin sphere is essentially symmetric, indicating no directional bonding.

The charge density distribution for NaCl-type ScS in the conduction band region (Figure 1.16) shows 3 bonding features. They are:

a) The absolute maximum of 0.0147 electrons/(a.u.)^3 is located at the center of the plot plane which is also at the center of a triangular face of the sulfur polyhedron. The lobes of the metal t_{2g} orbitals are directed toward the eight octahedral faces to form an indirect metal-metal bond network which mediates the metallic conductivity.

b) The charge density contours decrease less rapidly in the direction towards the nearest neighbor metal atoms out along the edge of the octahedron (0.0045 electrons/(a.u.)^3). This is the metal-metal t_{2g} σ-bond network.

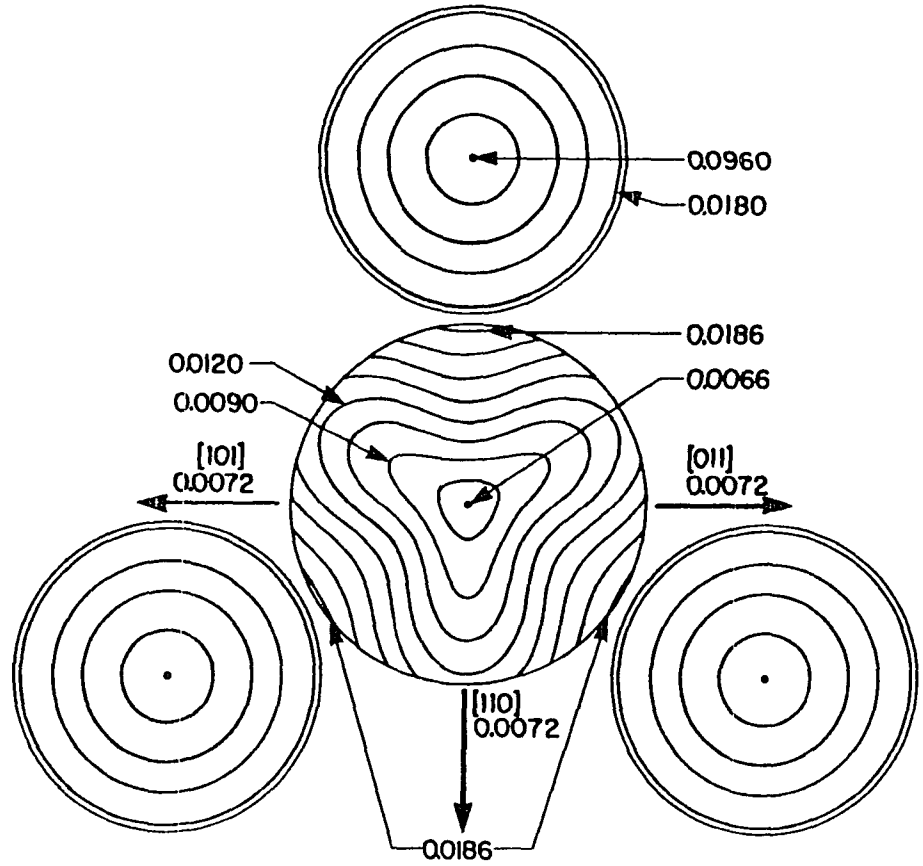

Figure 1.15. Valence band electron density for NaCl-type ScS in a plane perpendicular to the [111] direction. The plot plane slices the Sc muffin tin sphere (large circle in center) and three S muffin tin spheres (small circles)

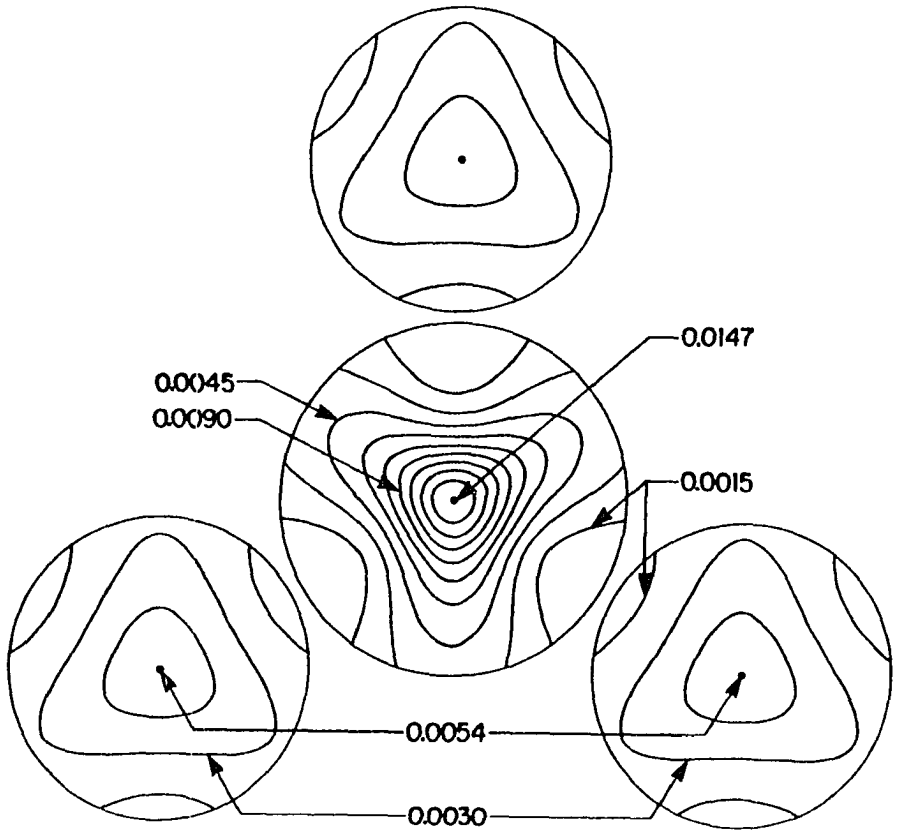

Figure 1.16. Conduction band electron density for NaCl-type ScS in a plane perpendicular to the [111] direction. The plot plane slices the Sc muffin tin sphere (large circle in center) and three S muffin tin spheres (small circles)

c) The charge density contours decrease more rapidly in the direction towards neighboring nonmetal atoms that form the octahedral cage about the central metal atom (0.0015 electrons/(a.u.)^3). This illustrates the minor role of metal t_{2g}-nonmetal p π-bonding in the conduction band region.

These three bonding interactions in the conduction band region, namely, the indirect metal-metal interaction directed through the octahedral faces, the direct metal-metal interaction directed through the octahedral edges and the metal-nonmetal π-bonding, are also present in NaCl-type ZrS[1] (Figure 1.17).

For Sc_3S_4, the charge distribution in a plane perpendicular to the [111] direction and in the valence band region is quite similar to that in ScS, mainly metal e_g-nonmetal p σ-bonding (Figure 1.18). A noticeable difference is the decrease in the amount of σ-bonding to the octahedral sulfur (0.0138 electrons/(a.u.)^3) and an increased σ-bonding interaction with the square planar sulfur atoms (0.0234 electrons/(a.u.)^3). An average charge density of 0.0202 electrons/(a.u.)^3 (vs. 0.0186 electrons/(a.u.)^3 in ScS) directed from the Sc atom toward the neighboring S atoms suggests an enhancement in covalency when vacancies are introduced into the metal sublattice. This result is consistent with the absence of a scandium core level energy shift in the nonstoichiometric material.

The three-fold symmetry of the charge density inside the Sc muffin tin sphere is also destroyed in Sc_3S_4 due to nonequivalent sulfur atoms comprising an octahedral face. In the conduction band region

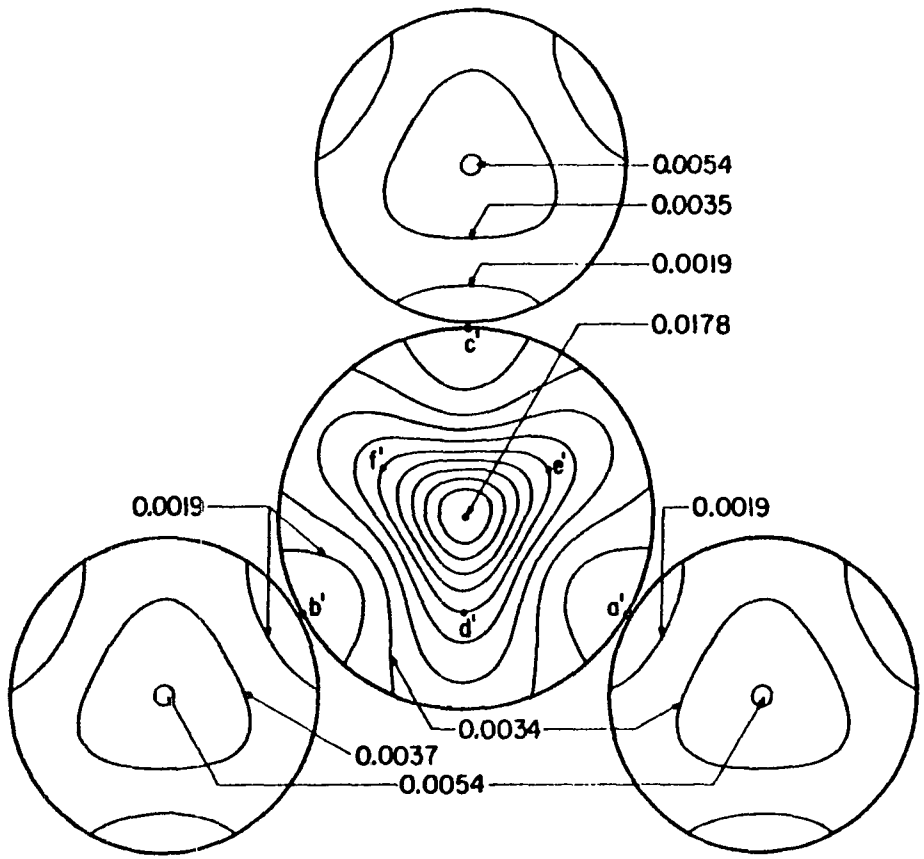

Figure 1.17. Conduction band electron density for NaCl-type ZrS in a plane perpendicular to the [111] direction. The points a', b' and c' denote the location at which the plot plane intersects the Zr-S bond axes. The points d', e' and f' denote the location at which the plot plane intersects the Zr-Zr bond axes

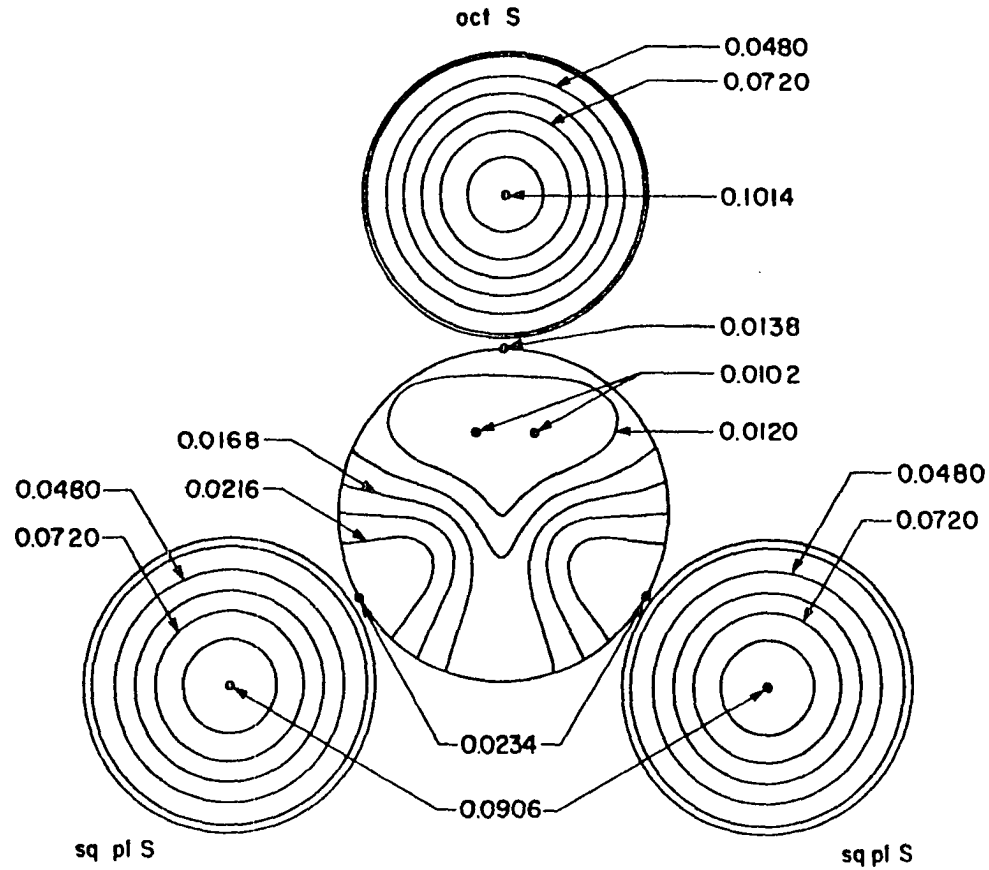

Figure 1.18. Valence band electron density for Sc_3S_4 in a plane perpendicular to the [111] direction. The plot plane slices the Sc muffin tin sphere (large circle in center) and three S muffin tin spheres

(Figure 1.19), the charge density maximum (0.0247 electrons/(a.u.)^3) is again directed through the octahedral face of the sulfur polyhedron but displaced in the direction towards the remaining 2 nearest neighbor Sc atoms. Despite the presence of metal atom vacancies, metallic conduction still mediates through this indirect metal-metal bond network. The charge density contours decrease less rapidly in the direction towards the remaining 2 nearest neighbor Sc atoms (e.g., 0.0080 electrons/(a.u.)^3), to form the usual metal-metal t_{2g} σ-bond network. Metal t_{2g}-nonmetal p π-bonding continues to exist as a minor component. A residual amount of charge (0.0028 electrons/(a.u.)^3) is now directed from Sc towards the vacancy.

The charge density contours inside the vacancy muffin tin sphere are forced to be spherically symmetric since only the contribution from the (0,0) component is taken into account. Evaluation of the charge density at the muffin tin boundary gave: 0.0069 electrons/(a.u.)^3 for the valence band region and 0.0002 electrons/(a.u.)^3 for the conduction band region.

The most prominent changes in the charge density when vacancies are introduced in the metal sublattice can be summarized as follows:

a) The charge density maximum in the conduction band region is displaced towards the remaining 2 nearest neighbor scandium atoms but nevertheless through the triangular faces of the sulfur polyhedron,

b) the marked decrease in the Sc-octahedral S σ-bonding interaction in the valence band region, and

c) the enhancement in the Sc-square planar S σ-bonding interaction in the valence band region, giving rise to an overall gain in covalency.

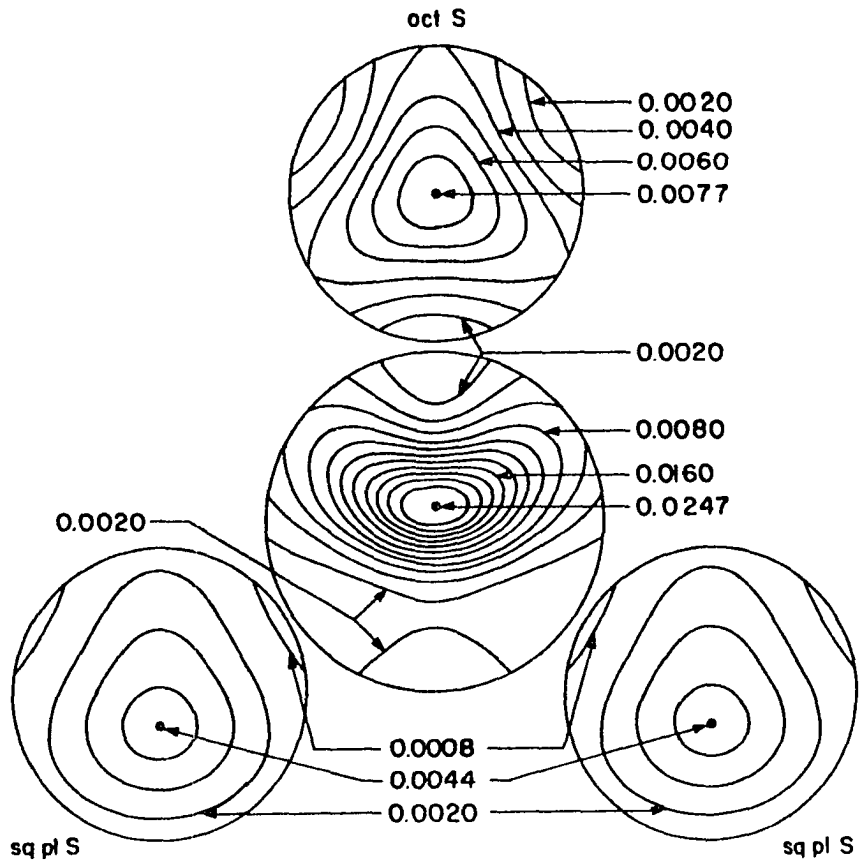

Figure 1.19. Conduction band electron density for Sc_3S_4 in a plane perpendicular to the [111] direction. The plot plane slices the Sc muffin tin sphere (large circle in center) and three S muffin tin spheres

DISCUSSION

The electronic structures of ScS and Sc_3S_4 were calculated using the Green's function KKR method to illuminate the influence of metal atom vacancies on the distribution of quantized electron states in the solid state and the changes in the character of the chemical bonds. From the results of rigorous quantum mechanical calculations, the creation of metal atom vacancies leads to:

a) a redistribution of sulfur wavefunctions near a vacancy site, creating nonbonding p-states, and

b) a decrease in the energy gap between the S 3p - Sc 3d valence band and the Sc 3d conduction band, increasing the overlap of S 3p and Sc 3d states.

The enhanced hybridization in Sc_3S_4 is therefore a possible explanation for the absence of change in the valency of Sc. From the charge density analysis, no new bonds are formed when vacancies are created; accommodating slight redistributions in the charge density but preserving the metal-nonmetal bonding interaction in the valence band region and the metal-metal bonding interaction in the conduction band region.

The electronic contribution to the specific heat has been measured for a near stoichiometric sample, $Sc_{0.99}S$.[23] The value of γ was 3.4 mJ/mol K^2 which corresponds to a DOS at the Fermi level of 20.1 states/primitive cell·Ry, compared to 14.0 states/primitive cell·Ry determined from the ScS calculation. The difference could be attributed to an

electron-phonon coupling and correlates well with the occurrence of superconductivity below 4.3 K.[24]

The theoretically derived energy dispersion curve for stoichiometric ScS can be compared with the optical spectrum measured by Zhuze and coworkers.[25] The peaks in the optical spectrum is due to electron transitions, direct or indirect (i.e., phonon assisted), from one band at low energy to another band at higher energy and the peak position is a measure of the interband energy difference at a certain wave vector $\vec{k}$. The experimental interband energy difference is then compared to the theoretical energy difference at the same wave vector $\vec{k}$. The reflection spectrum for ScS contained 4 peaks which were assigned as follows: the two peaks at low energies were due to transitions from the two maxima in the valence band region to the conduction band near the Fermi level, the third peak was due to the transition from the occupied L_2' to the empty L_3' state and the fourth peak was due to the transition from the sulfur 3s state to the conduction band near the Fermi level. Table 1.2 lists the experimental interband energy and the theoretically derived value. The closeness of these energy differences indicates that the theoretical model is reliable.

The mechanism for vacancy stabilization in $Sc_{1-x}S$ is probably energetic due to the large vacancy concentration, but the results of the electronic structure calculations cannot reveal the details of the mechanism. When vacancies are introduced into the solid, the Fermi level is lowered as was the general consensus but there were no localized defect states with accumulation of electron charge at the vacancy site as

Table 1.2. Comparison of the interband transition energy for stoichiometric ScS

Interband transition	Experiment[a] (Ry)	Theory[b] (Ry)
higher lying p-band region to E_f	0.301	0.301
deeper lying p-band region to E_f	0.433	0.480
L_2' to L_3'	0.654	0.660
sulfur 3s to E_f	1.015	0.981

[a]Reference 25.

[b]This work.

proposed by Huisman et al.,[11] there was a redistribution of electron states in the vicinity of a vacancy contrary to the rigid band prediction of Denker[26] and the d-band was narrower instead of broader as proposed by Goodenough.[27]

REFERENCES CITED

1. Nguyen, T.-H. Ph.D. Dissertation, Iowa State University, Ames, IA, 1980.

2. Merrick, J. A. Ph.D. Dissertation, Iowa State University, Ames, IA, 1980.

3. England, W. B.; Liu, S. H.; Myron, H. W. J. Chem. Phys. 1974, 60, 3760.

4. Nakahara, J.; Franzen, H.; Misemer, D. K. J. Chem. Phys. 1982, 76, 4080.

5. Ern, V.; Switendick, A. C. Phys. Rev. 1965, 137, 202.

6. Schwarz, K.; Ripplinger, H.; Neckel, A. Z. Phys. B 1982, 48, 79.

7. Gubanov, V. A.; Kurmaev, E. Z.; Ellis, D. E. J. Phys. C 1981, 14, 5567.

8. Neckel, A.; Rastl, P.; Eibler, R.; Weinberger, P.; Schwarz, K. J. Phys. C 1976, 9, 579.

9. Wimmer, E.; Schwarz, K.; Podloucky, R.; Herziq, P.; Neckel, A. J. Phys. Chem. Solids 1982, 43, 439.

10. Ivanovsky, A. L.; Gubanov, V. A.; Shveikin, G. P.; Kurmaev, E. Z. J. Less-Common Metals 1981, 78, 1.

11. Huisman, L. M.; Carlsson, A. E.; Gelatt, C. D.; Ehrenreich, H. Phys. Rev. B 1980, 22, 991.

12. Klima, J. J. Phys. C 1979, 12, 3691.

13. Klein, B. M.; Papaconstantopoulos, D. A.; Boyer, L. L. Phys. Rev. B 1980, 22, 1946.

14. Ries, G.; Winter, H. J. Phys. F 1980, 10,1.

15. Klima, J. Czech. J. Phys. B 1980, 30, 905.

16. Höchst, H.; Bringans, R. D.; Steiner, P.; Wolf, Th. Phys. Rev. B 1982, 25, 7183.

17. Porte, L.; Roux, L.; Hanus, J. Phys. Rev. B 1983, 28, 3214.

18. Köhn, W.; Rostoker, N. Phys. Rev. 1954, 94, 1111.

19. Mattheiss, L. F. Phys. Rev. 1963, 133, 184.

20. Hedin, L.; Lundqvist, B. I. J. Phys. C 1971, 4, 2064.

21. Jepsen, O. P.; Andersen, O. K. Solid State Commun. 1971, 9, 1763.

22. Franzen, H. F.; Anderegg, J. W., Ames Laboratory, private communication.

23. Moodenbaugh, A. R. Ph.D. Dissertation, University of California, San Diego, CA, 1975.

24. Moodenbaugh, A. R.; Johnston, D. C.; Viswanathan, R.; Shelton, R. N.; DeLong, L. E.; Fertig, W. A. J. Low Temp. Phys. 1978, 33, 175.

25. Zhuze, V. P.; Golubkov, A. V.; Karin, M. G.; Sidorin, K. K.; Shelykh, I. A. Sov. Phys. Solid State 1982, 24, 577.

26. Denker, S. P. J. Less-Common Metals 1968, 14, 1.

27. Goodenough, J. B. Phys. Rev. B 1972, 5, 2764.

SECTION II. HIGH TEMPERATURE VAPORIZATION OF SCANDIUM MONOSULFIDE

INTRODUCTION

The high temperature vaporization study of nonstoichiometric scandium sulfide by computer automated mass loss Knudsen effusion experiments was performed to investigate the energetics of vacancy formation. By determining the enthalpy changes associated with the vaporization reactions of the congruently subliming and stoichiometric monosulfides, the energy required to create approximately 20% scandium vacancies in ScS can be reaccessed, as well as the relative thermodynamic stabilities of these compounds.

An earlier study by Tuenge et al.[1] on the scandium-sulfur system employed both mass spectrometry and target collection Knudsen effusion techniques to determine the existence of a congruently subliming phase, to identify the vapor phase species and to obtain basic thermodynamic quantities for the vaporization reactions. Tuenge found that $Sc_{0.8065}S$ vaporized congruently over the temperature range 1875-2000 K and the mass spectrometric results established the vaporization processes as

$$Sc_{0.8065}S(s) = 0.8065\ Sc(g) + S(g) \qquad (2.1)$$

and

$$Sc_{0.8065}S(s) = 0.8065\ ScS(g) + 0.1935\ S(g). \qquad (2.2)$$

Second-law enthalpies at 298 K from target collection were ΔH°_{298} = 222.0 ± 4.0 kcal mol^{-1} for reaction 2.1 and ΔH°_{298} = 130.3 ± 4.0 kcal mol^{-1} for reaction 2.2. Third-law enthalpies at 298 K from mass spectrometry were ΔH°_{298} = 223.4 ± 4.5 kcal mol^{-1} for reaction 2.1 and ΔH°_{298} = 133.8 ± 4.5 kcal mol^{-1} for reaction 2.2. The third-law enthalpy change at absolute zero for the dissociation of ScS(g) was

calculated to be 110.0 ± 4.8 kcal mol^{-1}, which is in good agreement with those reported by Coppens, Smoes and Drowart[2] (D_0° = 113.4 ± 2.5 kcal mol^{-1}) and by Steiger[3] (D_0° = 113.5 ± 3.0 kcal mol^{-1}) from mass spectrometric investigations.

By performing a mass spec run from the stoichiometric monosulfide to the congruently vaporizing composition at 2035 K, thermodynamic properties of stoichiometric $Sc_{1.00}S$ were also obtained by Tuenge. These were:

$$ScS(s) = Sc_{0.8065}S(s) + 0.1935\ Sc(g), \qquad (2.3)$$
$$\Delta H^\circ_{298} = 18.3 \pm 2 \text{ kcal mol}^{-1}$$
$$ScS(s) = Sc(g) + S(g), \qquad (2.4)$$
$$\Delta H^\circ_{298} = 240.3 \pm 3 \text{ kcal mol}^{-1}$$

and

$$Sc(s) + S(s) = ScS(s), \qquad (2.5)$$
$$\Delta H^\circ_{298} = -82.8 \pm 3.5 \text{ kcal mol}^{-1}.$$

Reaction 2.3 describes the integral net process for the incongruent vaporization of ScS(s), and ΔH°_{298} for this process is a measure of the energy required to create vacancies in the stoichiometric monosulfide. Reaction 2.4 describes the atomization process which provides a measure of the cohesive energy of the stoichiometric solid and reaction 2.5 describes the standard formation process.

The primary goal of this vaporization study was to monitor the partial pressures of the effusing vapor species via the total mass loss as a function of temperature and composition. In addition to this, the temperature dependence of the activity of ScS across the homogeneity range of the monosulfide could be determined, as well as the thermodynamic properties of $Sc_{1.00}S(s)$.

EXPERIMENTAL

Sample Preparation and Characterization

The metal-rich scandium monosulfides were prepared by directly combining pieces of scandium foil (Ames Laboratory) and sulfur (Alfa Ventron, 99.999% purity) in a typical molar Sc to S ratio of 1.15 to 1.00. In addition, a small amount of $TeCl_4$ was added as a transport agent. The Sc, S and $TeCl_4$ were sealed in an evacuated fused silica ampoule and heated for several weeks in a tube furnace, initially at 450°C and eventually up to 800°C. When all the S had reacted, the scandium pieces were coated with yellow or green sesquisulfide. The samples were homogenized by annealing in an inductively heated W Knudsen cell at 1450°C in vacuum. The resulting material had a rich metallic gold luster and was easily powdered.

The composition was determined by combustion analysis: a weighed portion of $Sc_{1+x}S$ was oxidized in air to Sc_2O_3, at 900°C in a muffle furnace. The molar Sc to S ratio was obtained to within ±0.005 using 50-60 mg portions of sample. The lattice parameter was also obtained by taking an X-ray powder diffraction pattern (Guinier-Hägg camera using Cu $K\alpha_1$ radiation and NBS silicon internal standard). The cubic lattice parameter was plotted against the composition to yield the graph in Figure 2.1. It is significantly different from that obtained by Tuenge et al.[1] and Moodenbaugh,[4] who mainly studied the sulfur-rich monosulfides. Metallographic analyses of the Sc-rich monosulfides indicated a single phase, rather than a mixture of ScS and Sc metal.

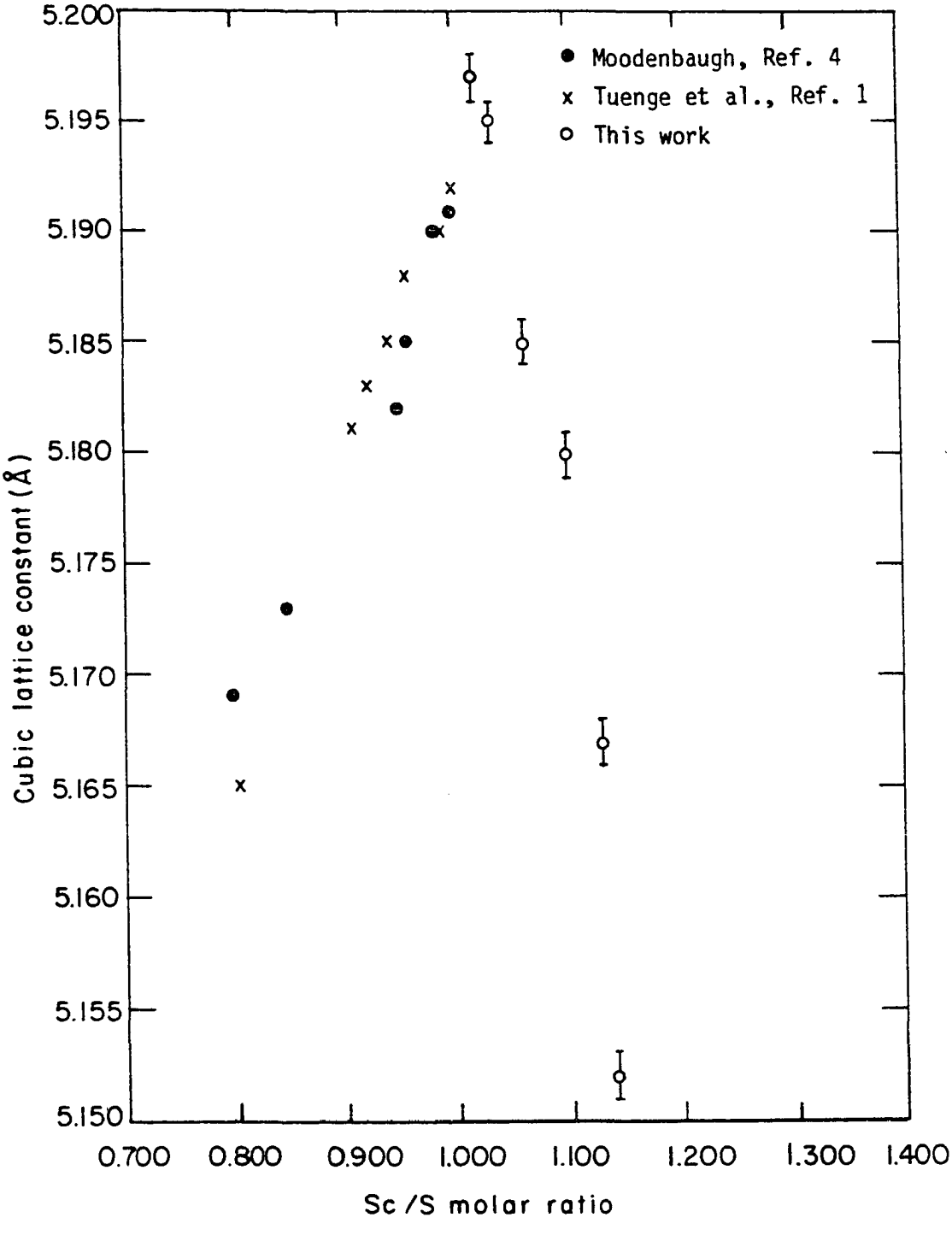

Figure 2.1. Composition vs cubic lattice parameter

The observed contraction of the lattice parameter deviating from the one-to-one composition could be explained in terms of vacancies. In the one-to-one compound there are no vacancies and the cell volume is maximized. However, when vacancies are randomly created in either sublattice ($Sc_{1+x}S$ and $Sc_{1-x}S$) the cell volume contracts giving rise to a smaller lattice constant. The existence of a metal-rich scandium monosulfide (i.e., $Sc_{1+x}S$) with sulfur vacancies has not previously been verified. By performing the high temperatuare vaporization experiments the question of metal solubility in ScS can be addressed.

Mass Loss Knudsen Effusion Experiments

Mass loss measurements were accomplished by using an instrument developed in the High Temperature Chemistry group by Anderegg, Kematick, Schiffman and Franzen. This instrument utilizes a MINC-11 microcomputer interfaced to a Cahn-RH microbalance and a Leeds and Northrup Electromax temperature controller. In addition, a UTI 100C 2-400 amu quadrupole mass spectrometer was used to monitor the effusate. A schematic diagram of the simultaneous mass loss-mass spec apparatus is shown in Figure 2.2. The computer software to obtain synchronous mass readings, temperature and ion currents from the effusing Knudsen cell was developed by Kematick and coworkers.[5]

About 55-75 mg of a scandium-rich monosulfide was placed in 3 semitoroidal tungsten liners and contained in a tungsten Knudsen cell with a knife-edge orifice at the bottom. The cell, suspended from the microbalance, was heated by radiation from a Sylvania tungsten mesh

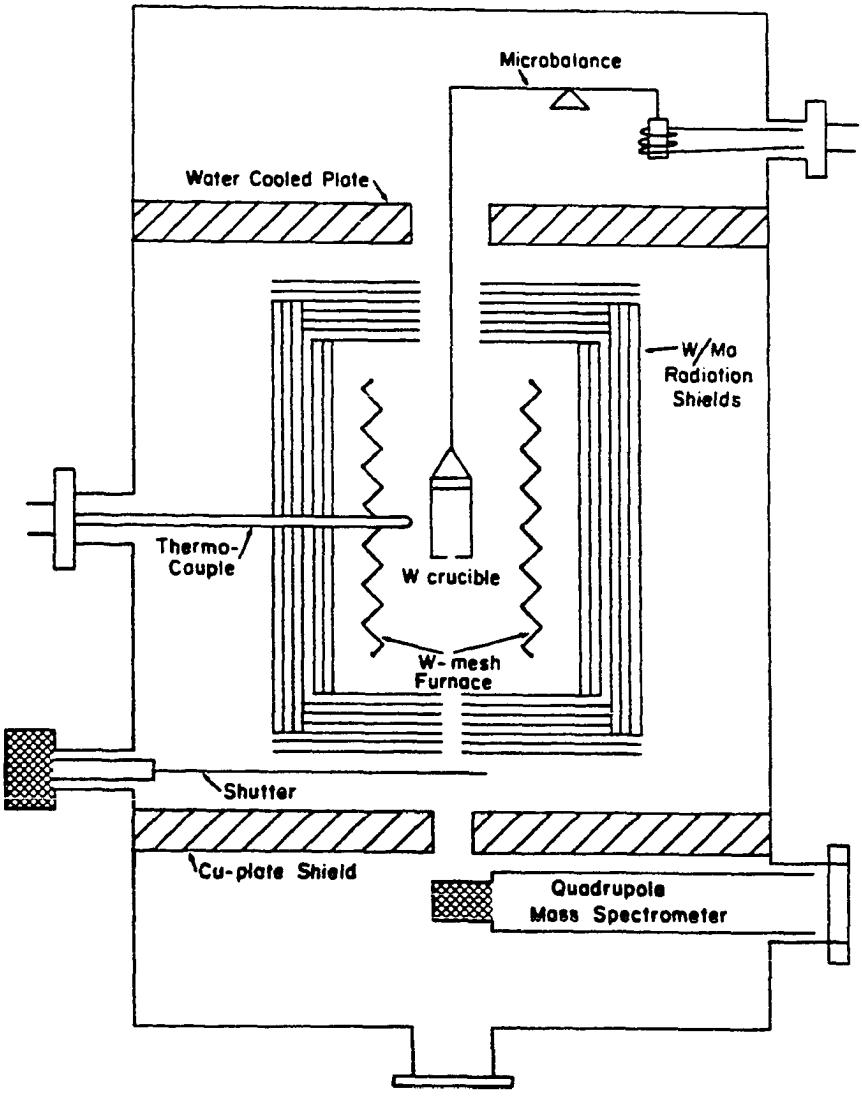

Figure 2.2. Schematic diagram of the simultaneous mass loss-mass spec apparatus

resistance furnace. The temperature of the cell was measured by a Ta sheathed, BeO insulated, W/5% Re - W/26% Re ARI Industries thermocouple, with the junction located within 1/4" from the Knudsen cell. This thermocouple was previously calibrated against another thermocouple suspended vertically into a dummy cell in order to correct for any temperature gradient that may exist between the cell and the tip of the thermocouple. The main assembly, consisting of the Knudsen cell, microbalance, mass spec, thermocouple and heater, was contained in a water cooled stainless steel chamber and evacuated to 10^{-7} torr by means of a diffusion pump.

The effusing vapor species were directed towards the mass spectrometer located below the furnace. Ion intensities at 45, 77 and 61 amu were measured corresponding to Sc^+, ScS^+ and ScO^+, respectively. The ion intensity was the difference between integrated signal averaged peak areas with the shutter open and closed.

Three runs employing the identical Knudsen cell (orifice area = 6.02 x 10^{-3} cm^2) and starting material ($Sc_{1.14}S$) were performed. Prior to data collection, the crucible and sample were annealed for approximately 24 hours at 1273 K. The temperature was then increased to that of the first isotherm (see Table 2.1) for a variable length of time from run to run. Time, temperature, balance reading, total mass loss and net ion currents of Sc, ScS and ScO were stored on a floppy disk and printed. The mass loss was also recorded on a strip-chart. When the rate of mass loss and the Sc ion current had decreased dramatically the temperature was increased. The congruently vaporizing composition was attained when

Table 2.1. Conditions before reaching the congruently vaporizing composition

Run	Isotherms
9	1610 K, 1906 K, 2103 K
10	1709 K, 1957 K
11	1609 K, 1756 K, 2053 K

the ion currents for Sc were constant with mass loss and the total mass loss was in excess of the calculated value. At this point, the temperature was increased to about 2100 K to vaporize the scandium that had condensed on the tantalum heat shields during the incongruent vaporization. The temperature was maintained at 2100 K for a few hours until the Sc ion current had once again become constant.

At the congruently vaporizing composition, rates of mass loss as a function of temperature were measured. The rate of mass loss was calculated at each temperature by using the computer generated data of time and balance reading.

THEORY

Calculation of the Thermodynamic Quantities of $Sc_{0.8065}S(s)$

Congruently subliming $Sc_{0.8065}S$ in equilibrium with its vapor is a chemical system comprised of 2 components and 2 phases, together with a composition constraint (i.e., the composition of the solid and vapor are the same). Consequently, applying the Gibbs phase rule

$$F = C - P + 2 \tag{2.6}$$

results in a univariant system. This means that if the temperature is specified then the partial pressures of the effusing vapor species are fixed, precisely in accordance with the thermodynamic equilibrium constant. In order to obtain vapor pressure measurements over $Sc_{0.8065}S$, rates of mass loss as a function of temperature were measured.

The mathematical relationship which describes the rate at which gas molecules effuse through a small (relative to the mean free path) orifice as a function of pressure, temperature and mass is given by the Knudsen equation,[6]

$$\frac{dm_i}{dt} = \frac{AP_iN_o}{(2\pi M_i RT)^{1/2}} \tag{2.7}$$

where

$\frac{dm_i}{dt}$ = mass rate at which gas molecules of the ith species escape in mg min^{-1}

A = orifice area in cm^2

P_i = partial pressure of the ith species in atm

N_o = Avogadro's number

M_i = molecular weight of the ith species in g mol^{-1}

R = gas constant in erg $mol^{-1}K^{-1}$

T = absolute temperature.

In the mass loss Knudsen effusion method, the vapor pressure of the gaseous species in equilibrium with the solid is calculated by measuring the total mass loss as a function of temperature,

$$\frac{\Delta m}{\Delta t} = \sum_{i}^{\text{no. species}} \frac{dm_i}{dt}$$

$$= \frac{A\ (cm^2)}{3.76\times10^{-7}\ T^{1/2}} \sum_{i} \frac{P_i\ (atm)}{(M_i(g\ mol^{-1}))^{1/2}}, \qquad (2.8)$$

where the value of 3.76×10^{-7} incorporates several constants. Applying equation 2.8 to the vaporization of $Sc_{0.8065}S(s)$, yields

$$\text{Rate } (mg\ min^{-1}) = \frac{A\ (cm^2)}{3.76\times10^{-7}\ T^{1/2}} \left[\frac{P_{Sc}}{M_{Sc}^{1/2}} + \frac{P_{ScS}}{M_{ScS}^{1/2}} + \frac{P_S}{M_S^{1/2}} \right]. \qquad (2.9)$$

The vapor in equilibrium with the condensed phase is, to a high degree of precision, ideal at the high temperatures and low pressures of these studies. The resulting thermodynamic equilibrium constant expression, therefore, involves only the partial pressures and not the fugacities of the vapor species. Combining the definition of the change in the standard Gibbs free energy function at temperature T,

$$\Delta G_T^\circ = \Delta H_T^\circ - T\Delta S_T^\circ \qquad (2.10)$$

with the equilibrium expression,

$$\Delta G^\circ_T = -RT \ln K \tag{2.11}$$

yields

$$R \ln K = - \frac{\Delta H^\circ_T}{T} + \Delta S^\circ_T \, . \tag{2.12}$$

Thermodynamic quantities like ΔH° and ΔS° referenced to a specific temperature can be obtained by either of 2 methods, the second- and third-law methods. The second-law enthalpy and entropy changes for a reaction have been frequently obtained by assuming that the heat capacities of the reactants and products are independent of temperature over the temperature range of the experiment. A plot of R ln K vs T^{-1} will be nearly linear, with the slope equal to the standard enthalpy change at the mean temperature, $-\Delta H^\circ_T$, and the intercept equal to the standard entropy change at the mean temperature, ΔS°_T. The resulting standard enthalpy and entropy changes at T are usually referenced to 0 K or 298 K, by using the standard enthalpy increments, $H^\circ_T - H^\circ_0$ or $H^\circ_T - H^\circ_{298}$, and the standard entropy increments, $S^\circ_T - S^\circ_0$ or $S^\circ_T - S^\circ_{298}$, for the reactants and products. The values of the enthalpy and entropy increments require estimates of C°_p of the reactants and products. An alternative procedure of the second-law method utilizes the change in the free energy function (Δfef) for the reaction and directly gives ΔH°_{298}. The change in the free energy function at temperature T is defined by

$$\Delta fef_T = (-\Delta G^\circ_T + \Delta H^\circ_{298})/T$$

$$= R \ln K + \frac{\Delta H^\circ_{298}}{T} \tag{2.13}$$

or

$$\Delta H^\circ_{298} = T(-R \ln K + \Delta fef_T) \qquad (2.14)$$

A plot of $(-R \ln K + \Delta fef_T)$ vs T^{-1} yields a line with the slope equal to ΔH°_{298}.

The third-law enthalpy change is the average value of ΔH°_{298} calculated from equation 2.14 for each temperature the mass loss was measured. The alternative second-law and third-law methods require that the fef of all the reactants and products be known as a function of temperature. For cases in which the fef has not been measured, it is necessary to estimate the fef using estimated heat capacities for the condensed phases (e.g., ScS(s) and $Sc_{0.8065}S(s)$) and using experimental spectroscopic data for the gas phase species (e.g., ScS(g)).

Thermal functions including the standard enthalpy and entropy increments and the standard fef's for ScS(s), $Sc_{0.8065}S(s)$ and ScS(g) were obtained from Tuenge,[7] Sc (g) from Hultgren et al.[8] and S(g) from the JANAF tables.[9]

RESULTS

Knudsen Effusion Vapor Pressure Measurements of $Sc_{0.8065}S(s)$

The partial pressures of Sc, ScS and S over the congruently vaporizing compound, corresponding to the 39 total mass loss data points, were calculated by solving three equations simultaneously. The first equation is the Knudsen effusion relation,

$$\text{Rate} = \frac{\Delta m}{\Delta t} = \frac{A}{3.76\times10^{-7}\ T^{1/2}} \left[M_{Sc}^{-1/2} P_{Sc} + M_{ScS}^{-1/2} P_{ScS} + M_{S}^{-1/2} P_{S}\right] \tag{2.15}$$

where $\Delta m/\Delta t$ = rate of total mass loss in mg min^{-1}, A = orifice area in cm^2, T = absolute temperature, M_{Sc}, M_{ScS} and M_S = molecular weights of Sc, ScS and S, respectively, in g mol^{-1}, and P_i = partial pressures in atm. The second equation is the material balance - congruence relation,

$$\frac{P_{Sc}}{M_{Sc}^{1/2}} + \frac{P_{ScS}}{M_{ScS}^{1/2}} = 0.8065 \left[\frac{P_S}{M_S^{1/2}} + \frac{P_{ScS}}{M_{ScS}^{1/2}} \right], \tag{2.16}$$

and the final equation is the thermodynamic equilibrium constant expression relating the equilibrium partial pressures,

$$K = \frac{P_{Sc}\ P_S}{P_{ScS}}. \tag{2.17}$$

The value of K evaluated at temperature T was calculated from the dissociation energy of ScS(g) at 0 K of 113.4 kcal mol^{-1}, reported by Coppens et al.[2] and the change in free energy function for the reaction

$$ScS(g) = Sc(g) + S(g). \tag{2.18}$$

The free energy functions for ScS(g) were taken from Tuenge,[7] while those

for Sc(g) and S(g) were obtained from Hultgren et al.[8] and the JANAF tables,[9] respectively. A linear least squares fit of ln K vs T^{-1} between 1500 K and 2500 K yielded

$$\ln K = -\frac{(57324 \pm 212)}{T} + (13.52 \pm 0.11), \qquad (2.19)$$

where the uncertainties are standard deviations.

The experimental data and the calculated partial pressures are listed in Table 2.2. The calculated results are also presented in Figure 2.3 as $\ln P_i$ vs T^{-1} for the individual partial pressures. Linear least squares fits to the data yielded

$$\ln P_{Sc} = -\frac{(63260 \pm 888)}{T} + (15.89 \pm 0.43), \qquad (2.20)$$

$$\ln P_{ScS} = -\frac{(69797 \pm 1868)}{T} + (18.70 \pm 0.90), \qquad (2.21)$$

$$\ln P_{S} = -\frac{(63864 \pm 980)}{T} + (16.33 \pm 0.47), \qquad (2.22)$$

where the uncertainties are standard deviations.

The resulting partial pressures were then used to calculate second-law enthalpy and entropy changes at the mean temperature according to equation 2.12 for the congruent vaporization reactions:

$$Sc_{0.8065}S(s) = 0.8065\ Sc(g) + S(g) \qquad (2.23)$$

$$Sc_{0.8065}S(s) = 0.8065\ ScS(g) + 0.1935\ S(g). \qquad (2.24)$$

The standard enthalpy and entropy changes for vaporization at the mean temperature (2100 K) and at 298 K are listed in Table 2.3. The enthalpy

Table 2.2. Total mass loss Knudsen effusion results

Temperature (K)	$\frac{\Delta m}{\Delta t} \times 10^{-3}$ (mg min^{-1})	$P_{Sc} \times 10^{-7}$ (atm)	$P_{ScS} \times 10^{-7}$ (atm)	$P_S \times 10^{-7}$ (atm)
2053	2.45	3.52	2.58	4.08
2143	7.66	11.3	8.18	13.1
2197	16.0	23.2	18.2	27.1
2074	3.06	4.49	3.14	5.19
2026	1.27	1.96	1.14	2.22
2169	10.6	15.7	11.4	18.2
2122	5.70	8.43	5.96	9.74
2124	6.87	9.70	7.80	11.4
2126	7.30	10.2	8.44	12.0
2027	1.60	2.33	1.61	2.69
2066	2.75	4.02	2.83	4.64
2006	1.03	1.56	0.949	1.78
2076	2.75	4.18	2.63	4.79
2151	9.70	13.7	11.1	16.1
2078	3.74	5.26	4.14	6.15
2110	5.66	8.02	6.33	9.37
2111	4.99	7.36	5.21	8.51
2054	2.70	3.78	2.97	4.42
2055	2.17	3.25	2.12	3.73
2153	9.86	14.0	11.3	16.4
2030	1.45	2.19	1.36	2.50
2129	6.39	9.38	6.80	10.9
2006	1.25	1.78	1.28	2.07
2073	3.46	4.88	3.80	5.70
2104	5.05	7.20	5.56	8.40
2055	2.15	3.22	2.09	3.70
2153	9.94	14.1	11.4	16.5
2030	1.43	2.17	1.33	2.48
2104	5.33	7.48	6.03	8.76
2055	2.53	3.63	2.67	4.21
2124	6.87	9.70	7.80	11.4
2025	1.32	2.01	1.22	2.29
2074	3.29	4.73	3.50	5.49
2001	0.892	1.37	0.793	1.55
2132	7.22	10.4	8.02	12.1
2045	2.08	3.03	2.12	3.50
2006	1.05	1.58	0.978	1.80
2105	5.14	7.35	5.65	8.56
2143	8.28	11.9	9.20	13.9

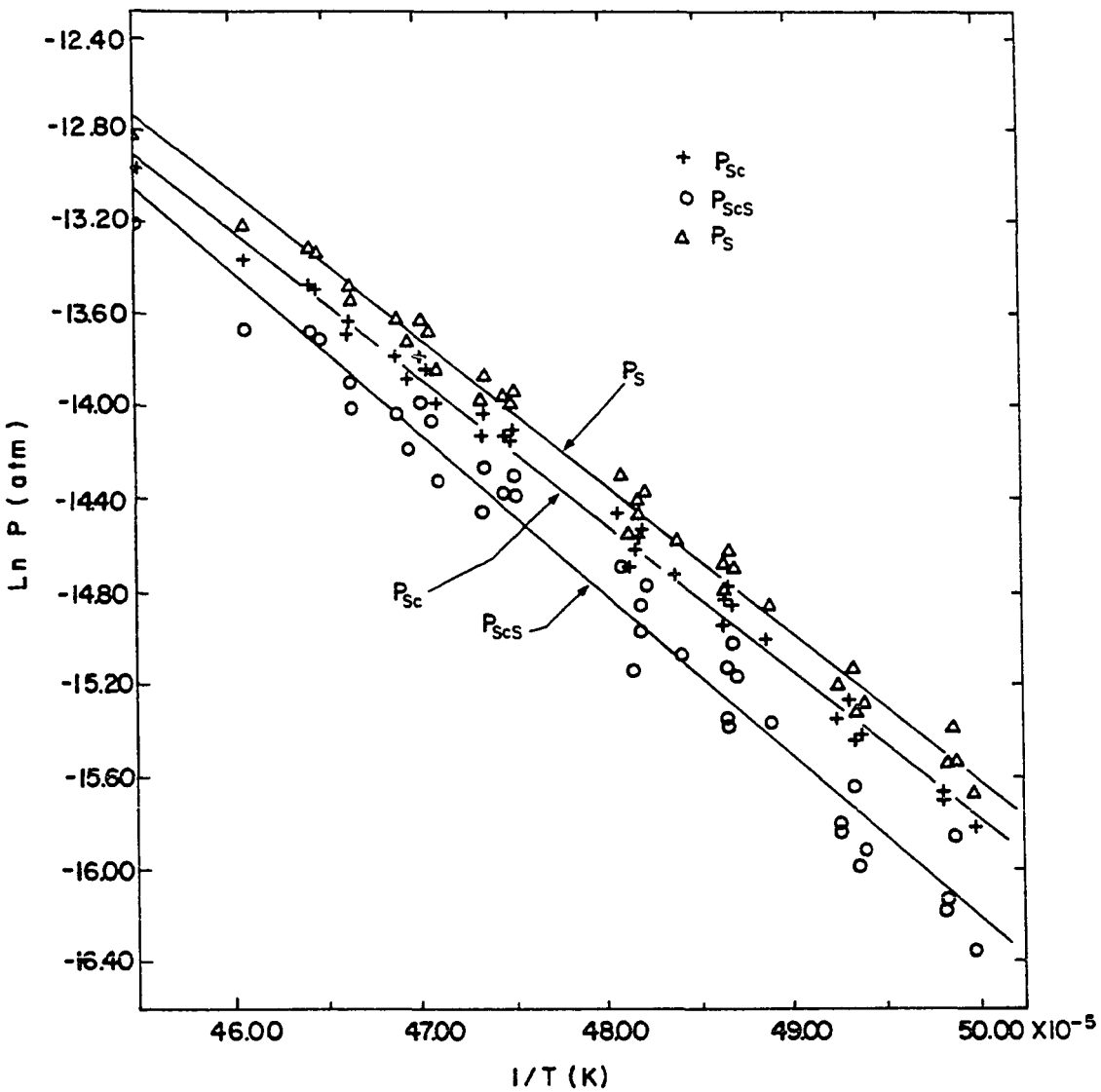

Figure 2.3. Ln P_i vs T^{-1} of four mass loss Knudsen effusion experiments at the congruently vaporizing composition, $Sc_{0.8065}S(s)$

Table 2.3. Second-law results for $Sc_{0.8065}S(s)$

Reaction	ΔH°_{2100} [a] (kcal mol^{-1})	ΔS°_{2100} [a] (cal mol^{-1} K^{-1})	ΔH°_{298} [b] (kcal mol^{-1})	ΔS°_{298} [b] (cal mol^{-1} K^{-1})
$Sc_{0.8065}S(s) = 0.8065\ Sc(g) + S(g)$	228.4±3.4	58.0±1.6	235.1±3.8	64.1±2.4
$Sc_{0.8065}S(s) = 0.8065\ ScS(g) + 0.1935\ S(g)$	136.4±3.4	36.3±1.6	144.8±3.8	44.8±2.4

[a]Uncertainties are standard deviations.

[b]Uncertainties are propagated from standard deviations and the uncertainties in enthalpy (±1 kcal mol^{-1}) and entropy functions (±1 cal mol^{-1} K^{-1}).

and entropy increments used to reduce ΔH°_{2100} and ΔS°_{2100} to 298 K are given in Table 2.4.

The alternative second-law and third-law methods which utilize the experimentally determined equilibrium constant and the estimated change in fef were used to calculate the enthalpy changes for the vaporization reactions of $Sc_{0.8065}S(s)$ at 298 K, according to equation 2.14. A plot of $(-R \ln K + \Delta fef_T)$ vs T^{-1} for each of the vaporization processes was generated which provided a slope equal to ΔH°_{298}. The third-law enthalpy change for reactions 2.23 and 2.24 was the average value of the term $T(-R \ln K + \Delta fef_T)$, calculated at each experimental data point. Table 2.5 lists the results.

Knudsen Effusion Vapor Pressure Measurements Between $Sc_{1.14}S(s)$ and $Sc_{0.8065}S(s)$

The mass vs time data for each of the 3 runs prior to reaching the congruently vaporizing composition are presented in Figures 2.4 - 2.6, at two or three different temperatures for a single run. The data were initially converted to dm/dt values, by estimating the slope of the mass vs time curves at 20 or 40 minute time intervals. The resulting slopes were then integrated using a linear approximation for the curved segments and the integrated mass loss was compared to the raw data. The initial guesses of the dm/dt values were improved by satisfying the following criteria: (a) the resulting integrated mass vs time data agreed with the raw data to within ± 0.05 mg, (b) the dm/dt values decreased with time during an isothermal vaporization and (c) the difference in consecutive dm/dt values decreased with time during an isothermal vaporization.

Table 2.4. Enthalpy and entropy increments

	Sc(g)[a]	ScS(g)[b]	S(g)[c]	$Sc_{0.8065}S(s)$[b]	ScS(s)[b]
$H^\circ_{2100} - H^\circ_{298}$ (kcal mol^{-1})	9.077	16.30	9.335	23.4	25.9
$S^\circ_{2100} - S^\circ_{298}$ (cal mol^{-1} K^{-1})	9.879	17.23	10.30	24.4	27.0
S°_{298} (cal mol^{-1} K^{-1})	41.75	56.65	40.09	11.8	12.7

[a]Reference 8.

[b]Reference 7.

[c]Reference 9.

Table 2.5. Second- and third-law results for $Sc_{0.8065}S(s)$

Reaction	ΔH°_{298}[a] (II)	ΔH°_{298}[b] (III)
$Sc_{0.8065}S(s) = 0.8065\ Sc(g) + S(g)$	233.6±3.4	230.7±1.8
$Sc_{0.8065}S(s) = 0.8065\ ScS(g) + 0.1935\ S(g)$	143.3±3.4	138.4±1.8

[a]Uncertainties are standard deviations.

[b]Uncertainties include standard deviations and the uncertainties in Δfef (±1 cal mol^{-1} K^{-1}).

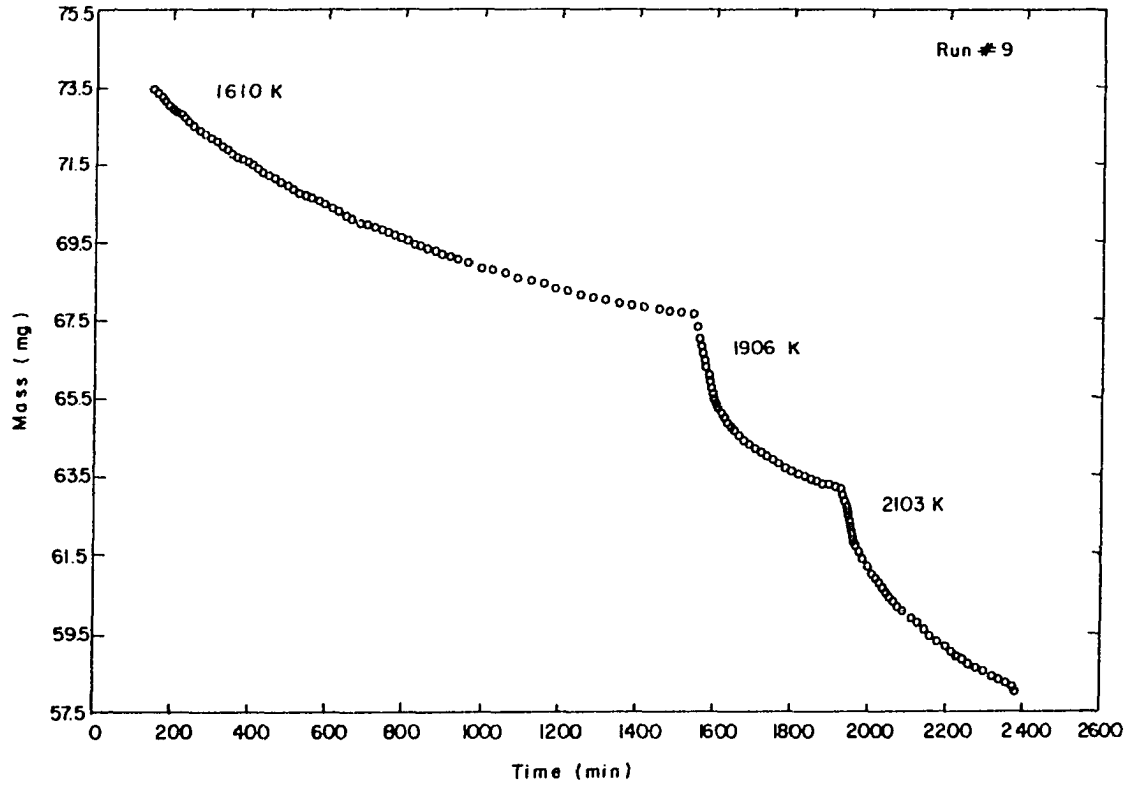

Figure 2.4. Mass vs time for run #9

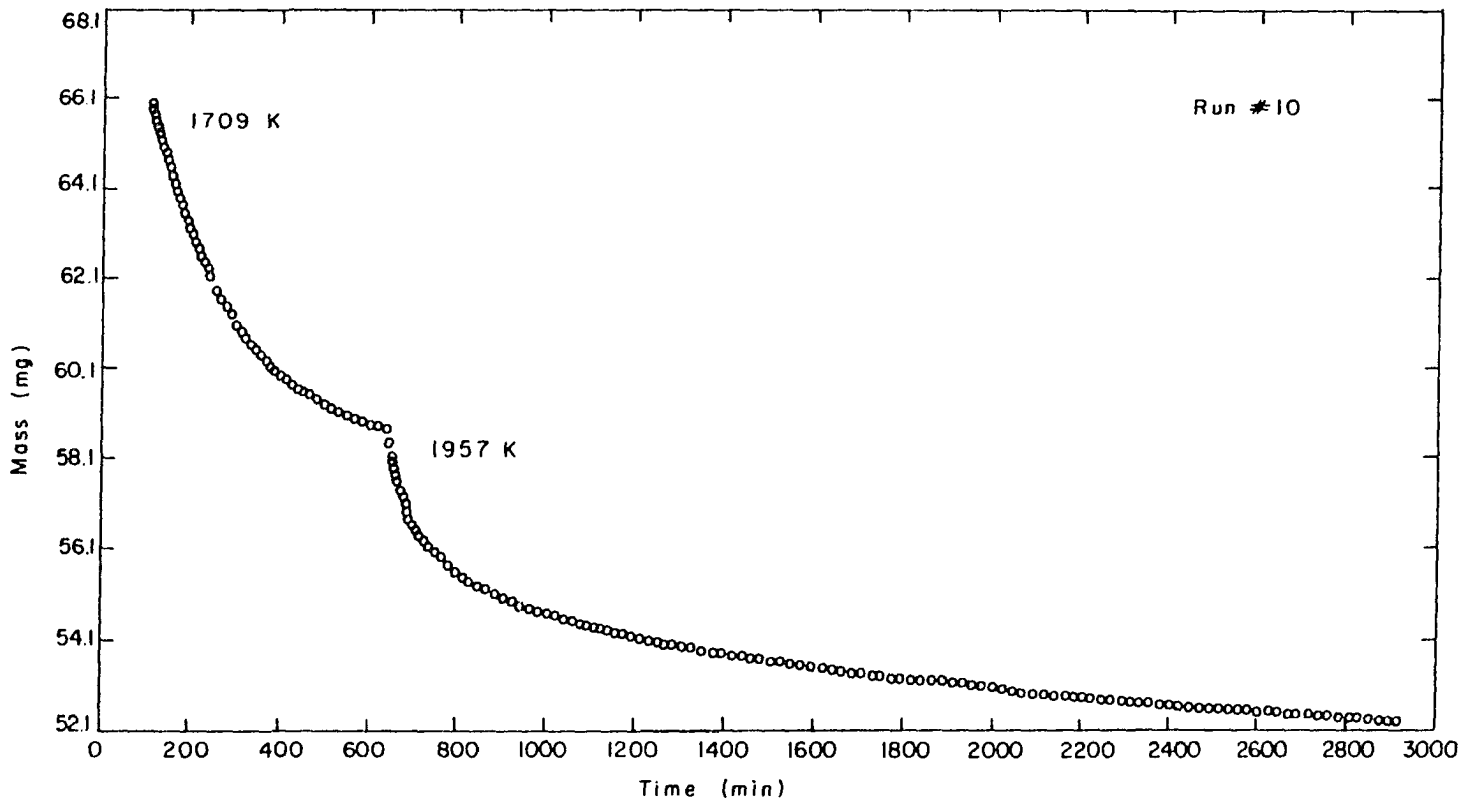

Figure 2.5. Mass vs time for run #10

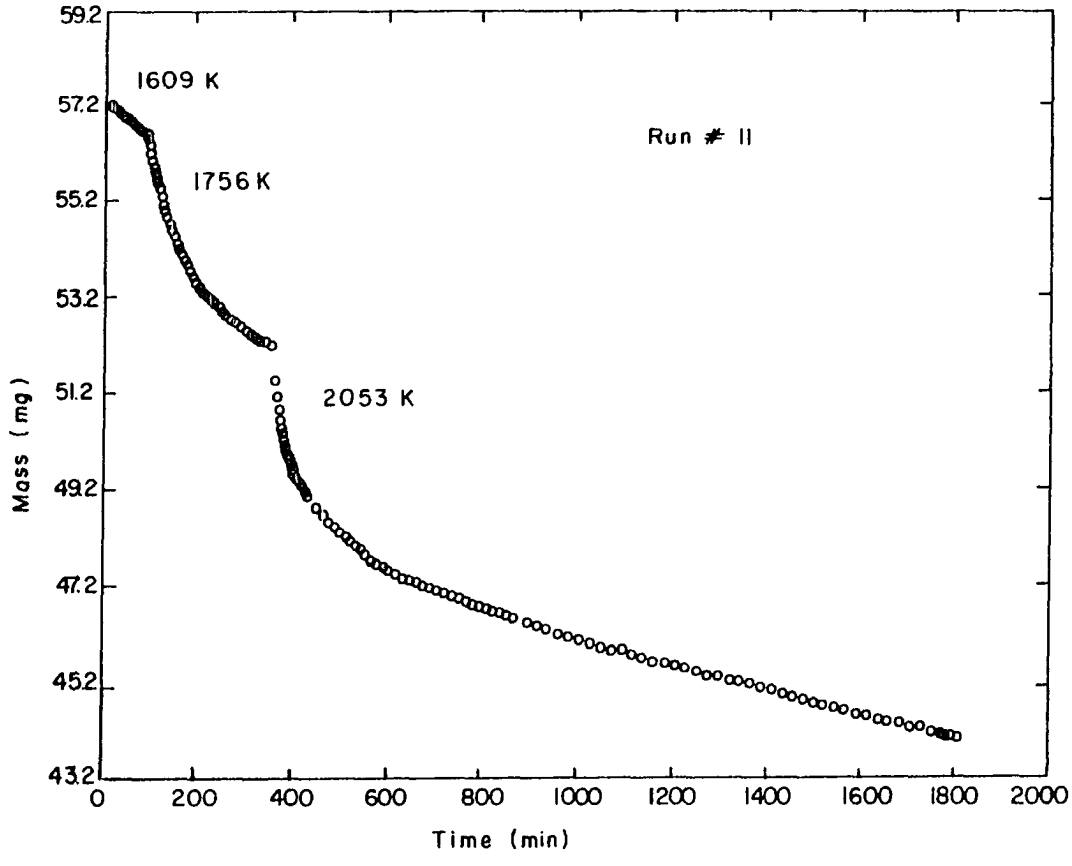

Figure 2.6. Mass vs time for run #11

The improved set of dm/dt values were then used to determine the partial pressures of S(g), Sc(g) and ScS(g) by the following procedure. Initial guesses of P_{Sc} were obtained at the temperature of the final isotherm for each run, each of which terminated with the congruently vaporizing compound (assumed to be $Sc_{0.8065}S^{1}$), by first subtracting the value of dm/dt at congruence from the dm/dt value at the start of the final isotherm. The difference was assumed to be solely Sc(g) and the corresponding P_{Sc} value was added to that for the congruently vaporizing composition, $P_{Sc,cong}$. These initial P_{Sc} values, together with the values for S(g) and ScS(g) at the congruently vaporizing composition ($P_{S,cong}$ and $P_{ScS,cong}$) were used to calculate the moles of Sc(g), S(g) and ScS(g) vaporized and hence the composition of Sc_xS over the duration of the final isotherm. These compositions (mole fractions, X_{Sc} and X_S) and initial P_{Sc} values were used to obtain an improved set of P_S values by employing the integral form of the Gibbs-Duhem equation

$$\ln \frac{P_S}{P_{S,cong}} = - \int_{cong}^{final\ state} \frac{X_{Sc}}{X_S} \, d \ln P_{Sc}. \qquad (2.25)$$

The integral was evaluated by using a piecewise linear approximation. The improved set of P_S and the initial P_{Sc} values were combined to calculate improved values of P_{ScS} according to the thermodynamic equilibrium constant expression (equation 2.17). The value of K at the temperature of the final isotherm was obtained by the linear least squares result (equation 2.19). The improved values of P_S and P_{ScS}

in turn provided better estimates for the S(g) and ScS(g) contributions to dm/dt. A new set of dm/dt values was generated by subtracting the S(g) and ScS(g) contributions from the starting dm/dt values, and the improved Sc(g) contribution to dm/dt was used to obtain a refined set of P_{Sc} values. This procedure was repeated for several iterations until no change in the sets of values of X_{Sc}, P_S, P_{Sc} and P_{ScS} were observed.

An explanation of the linear approximation of the integrals is perhaps necessary. The pertinent data (dm/dt vs time and X_{Sc}/X_S vs ln P_{Sc}) were plotted and the intervals along the abscissa were decreased if the area between a curve fitted to the data (by eye) and a straight line drawn across the interval could be determined. The coincidence of the linear segment and the curve drawn through the data, suggests that the linear integral approximations introduce negligible error in addition to those inherent in the experiment (about ±0.05 mg).

In order to obtain values for the partial pressures for a given composition but at a different temperature (i.e., at the time the temperature was changed from the original isotherm), it was assumed that a plot of ln P_{ScS} vs T^{-1} generated from the three P_{ScS} values at the final isotherms could be extrapolated. Extrapolation of a curve containing only 3 points might introduce appreciable error in P_{ScS}, however, at the compositions at which the isotherm changed, ScS(g) generally comprised less than 1% of the vapor, i.e., the vapor was 99% Sc(g), and thus negligible error should be introduced in P_{Sc}. The resultant error in P_{ScS} was compensated by finally using the same

value of the slope to back calculate the pressure of ScS(g) over the stoichiometric solid, P°_{ScS}, and at the temperature of the final isotherm.

Back calculating the starting composition, assuming that the composition at the end of the run was $Sc_{0.8065}S$, resulted in values very close to the composition determined analytically by combustion analysis: $Sc_{1.14}S$, $Sc_{1.16}S$ and $Sc_{1.13}S$ compared to the determined value of $Sc_{1.14}S$. The Sc(g) pressures calculated at the start of each run were approximately equal to the Sc vapor pressures reported in Hultgren et al.,[8] for example, 1.55×10^{-5} atm compared with 2.5×10^{-5} atm at 1709 K. The rapid decrease in P_{Sc} from the start of the run strongly indicates that the homogeneity range in the Sc-S system extends very close to $Sc_{1.14}S$, contrary to earlier findings by Tuenge and coworkers.[1]

From the calculations just described, a set of approximate values of P°_{ScS} evaluated over $Sc_{1.00}S(s)$ resulted. These results are in error because of the uncertainty in the composition and temperature dependence of P_{ScS}, and in particular because an approximate ln P_{ScS} vs T^{-1} slope has been used to determine boundary values of P_{ScS} for the lower temperature isotherms. In order to compensate for this approximation, the P°_{ScS} values were corrected to the temperature of the final isotherm using the same value of the slope ($d \ln P_{ScS}/dT^{-1} = -50 \times 10^3$ K), that was used to calculate the boundary values at the end of the isotherms. Table 2.6 lists the pertinent values.

Table 2.6. Vapor pressure of ScS in equilibrium with $Sc_{1.00}S(s)$ evaluated at the temperature of the final isotherm T_2

Run	$T_1(K)$ $Sc_{1.00}S$	$T_2(K)$ $Sc_{0.8065}S$	$P^{\circ}_{ScS}(T_1)$ (atm)	$P^{\circ}_{ScS}(T_2)$ (atm)	$P_{ScS,cong}(T_2)$ (atm)
9	1610	2103	6.89×10^{-10}	1.35×10^{-6}	6.33×10^{-7}
10	1709	1957	4.32×10^{-9}	1.76×10^{-7}	7.73×10^{-8}
11	1756	2053	6.81×10^{-9}	4.12×10^{-7}	2.17×10^{-7}

In order to calculate the enthalpy of formation of the monosulfide, $Sc_{1.00}S(s)$, from that of the congruently vaporizing phase, $Sc_{0.8065}S(s)$, the temperature dependence of the activity of ScS in $Sc_{0.8065}S(s)$ must be known. The activity of ScS, computed as $P_{ScS,cong}/P^{\circ}_{ScS}$, where P°_{ScS} is the vapor pressure of ScS in equilibrium with the stoichiometric $Sc_{1.00}S(s)$ and $P_{ScS,cong}$ is the vapor pressure of ScS in equilibrium with the congruently vaporizing composition at the same temperature, is 0.47 at 2103 K, 0.44 at 1957 K and 0.53 at 2053 K. These values demonstrate that within the experimental temperature range of 1950 K to 2100 K, there is no appreciable temperature trend of the activity of ScS in $Sc_{0.8065}S(s)$, i.e., $a_{ScS} = 0.48 \pm 0.05$.

The value of the activity can be used to determine the enthalpy change associated with the formation of vacancies in $Sc_{1.00}S(s)$:

$$ScS(s) = Sc_{0.8065}S(s) + 0.1935\ Sc(g) \qquad (2.26)$$

The above reaction is the result of the sum of the following two reactions:

$$ScS(g) = Sc_{0.8065}S(s) + 0.1935\ Sc(g) \qquad (2.27)$$

and

$$ScS(s) = ScS(g). \qquad (2.28)$$

For reaction 2.27, $\Delta G^\circ_T = -RT \ln \frac{P_{Sc}^{0.1935}}{P_{ScS}}$, where P_{Sc} and P_{ScS} are the partial pressures corresponding to the congruently vaporizing composition. For reaction 2.28, $\Delta G^\circ_T = -RT \ln P^\circ_{ScS}$. Therefore for reaction 2.26, $\Delta G^\circ_T = -RT \ln \frac{P_{Sc}^{0.1935} P^\circ_{ScS}}{P_{ScS}} = RT \ln \frac{a_{ScS}}{P_{Sc}^{0.1935}}$

$$= RT \ln a_{ScS} - 0.1935\ RT \ln P_{Sc}. \qquad (2.29)$$

Evaluating ΔG°_T from equation 2.29 and estimating ΔS°_T at the temperature of the final isotherm of each run yielded an estimated enthalpy change for reaction 2.26 which is independent of temperature, 22.2 ± 0.2 kcal mol^{-1} at a mean temperature of 2030 K. Table 2.7 lists the calculated ΔG°_T, the estimated ΔS°_T and the estimated ΔH°_T. Referencing the enthalpy change to 298 K yields 23.0 ± 1.7 kcal mol^{-1}. This value can be compared with that reported by Tuenge et al.,[1] 18.3 ± 2.0 kcal mol^{-1}. The 5 kcal mol^{-1} discrepancy could be due to the fact

Table 2.7. Thermodynamic quantities for the reaction ScS(s) = $Sc_{0.8065}S(s)$ + 0.1935 Sc(g)

T (K)	P_{Sc}^{a} (atm)	ΔG_T° (kcal mol^{-1})	ΔS_T° (cal mol^{-1} K^{-1})	ΔH_T° (kcal mol^{-1})
2103	6.87×10^{-7}	8.4	6.5	22.1
1957	7.28×10^{-8}	9.5	6.6	22.4
2053	3.30×10^{-7}	8.8	6.5	22.1

[a]Calculated from the linear least squares result for P_{Sc} over $Sc_{0.8065}S(s)$ (equation 2.20).

that Tuenge based his value on a single mass spectrometric experiment at 2035 K and that $Sc_{1.00}S(s)$ was saturated with Sc. It was furthermore discovered from the current vaporization experiments that the ion currents for Sc and ScS are suspect, due to the presence of Sc vapor species subliming from the radiation heat shields and the weak and oscillating net intensity from the ScS vapor species throughout the entire run.

A second method of determining the enthalpy change for reaction 2.26 does not require a knowledge of the value of the activity of ScS but only of its temperature independence. This method utilizes the Gibbs-Helmholtz equation, $\Delta H_T^\circ = \frac{d(\Delta G_T^\circ/T)}{dT^{-1}}$, and when applied to equation 2.29, we find that

$$\Delta H^\circ_T = -0.1935\ R \frac{d \ln P_{Sc}}{dT^{-1}} . \qquad (2.30)$$

Using the value of the slope of ln P_{Sc} vs T^{-1}, which was determined from the mass loss data at the congruently subliming composition (equation 2.20), gives ΔH°_{2100} = 24.3 ± 0.3 kcal mol^{-1} or ΔH°_{298} = 25.0 ± 1.8 kcal mol^{-1}. The latter value can be compared to that obtained by substituting Tuenge's value of the slope of ln P_{Sc} vs T^{-1} from the target collection data into equation 2.30, yielding 24.4 ± 1.7 kcal mol^{-1}. This closer agreement using the slope of ln P_{Sc} vs T^{-1} supports the previous paragraph that the mass spec results are suspect.

The atomization or cohesive energy of $Sc_{1.00}S(s)$ referenced to 298 K can be obtained by combining reactions 2.23 and 2.26 to give ΔH°_{298} = 255.7 ± 2.6 kcal mol^{-1}. The enthalpy of formation of $Sc_{1.00}S(s)$ at 298 K from scandium metal and sulfur can be obtained by combining the atomization enthalpy of $Sc_{1.00}S(s)$ with the vaporization enthalpies of Sc(s)[8] and S(s)[9] to give $\Delta H^\circ_{f,298}$ $[Sc_{1.00}S(s)]$ = -98.7 ± 2.8 kcal mol^{-1}. The enthalpy of formation of $Sc_{0.8065}S(s)$ at 298 K can be derived in the same manner to yield $\Delta H^\circ_{f,298}$ $[Sc_{0.8065}S(s)]$ = -91.2 ± 2.1 kcal mol^{-1}. Using the estimated entropy of formation of $Sc_{1.00}S(s)$ at 298 K of -3.2 ± 1.0 cal mol^{-1} K^{-1}, which is calculated from S°_{298} for Sc(s),[8] S(s)[9] and ScS(s),[7] together with the enthalpy of formation, yields a standard free energy of formation of $Sc_{1.00}S(s)$ at 298 K of -97.8 ± 2.8 kcal mol^{-1}.

DISCUSSION

The high temperature Knudsen effusion study by the total mass loss method was performed to reaccess the energy required to create approximately 20% vacant scandium sites in the monosulfide. The original plan was to simultaneously measure the Sc and ScS ion currents along with the total mass loss in order to determine the partial pressures of Sc, ScS and S as a function of both temperature and composition. In this manner, the calculation of the partial pressures would have been done in a straightforward manner, i.e., once the mass spec calibration constant was obtained for each vapor species, from the mass loss rates at the congruently vaporizing composition, all the partial pressures of Sc, ScS and S were known from the start of the run until the congruently vaporizing composition from the ion currents, rather than iterating the mass loss data. The ion currents were not used in this investigation to calculate thermodynamic functions and are presumed to be erroneous since at the higher temperatures sublimation of scandium from the heat shields was occurring and the effective Knudsen cell had a much larger orifice (at least 1/4" in diameter), therefore resulting in larger ion currents and partial pressures for Sc. A solution to this problem may be the addition of a more effective water cooling jacket in the vicinity of the heat shields outside the vacuum chamber. In addition, the ScS ion currents were so small and oscillatory, and sometimes even unshutterable, making it difficult to observe an increasing or decreasing trend in the partial pressure with composition at constant temperature.

Despite the experimental difficulties encountered in this investigation, several thermodynamic properties of $Sc_{1.00}S(s)$ were determined and the solubility of Sc metal in ScS to form a homogeneous compound was noted. The metal-rich end of the cubic single phase region was found to extend to $Sc_{1.14}S$ since there were no lines corresponding to hexagonal Sc metal in the X-ray powder pattern and the Sc partial pressure decreased rapidly at the start of a run (typically at 1300°C). Additional experiments using different starting compositions (i.e., more metal rich than $Sc_{1.14}S$) are required to firmly establish the width of the cubic single phase region.

The second law enthalpy changes at 298 K for the vaporization reactions of $Sc_{0.8065}S(s)$ (reactions 2.1 and 2.2) are approximately 15 kcal mol^{-1} larger than those reported by Tuenge et al.[1] using the target collection method. This large discrepancy could be due to the fact that the partial pressures of Sc, ScS and S were significantly smaller than those determined by Tuenge and the relative pressure trend was totally different (Tuenge: $P_{ScS} > P_S > P_{Sc}$; this work: $P_S > P_{Sc} > P_{ScS}$). The target collection data are probably less reliable because the crucible was not in an isothermal environment and an analytical spectroscopic determination of the concentration of the Sc species on the targets is not as accurate as is the direct measurement of mass.

From the temperature independent value of the activity of ScS in $Sc_{0.8065}S(s)$, $a_{ScS} = 0.48 \pm 0.05$, thermodynamic properties of $Sc_{1.00}S(s)$ were determined. The energy required to create approximately 20% scandium vacancies in $Sc_{1.00}S(s)$ at 298 K was found to be

25.0 ± 1.8 kcal mol^{-1}. This value is significantly smaller than that predicted by the ionic model, 132 kcal mol^{-1}, in which Sc is divalent in $Sc_{1.00}S(s)$ and a mixture of divalent and trivalent cations in $Sc_{0.8065}S(s)$. This result indicates that the ionic model fails to predict vacancy formation in $Sc_{1.00}S(s)$ at high temperatures. The atomization or cohesive energy at 298 K of $Sc_{1.00}S(s)$ was 255.7 ± 2.6 kcal mol^{-1} and the enthalpy of formation at 298 K was -98.7 ± 2.8 kcal mol^{-1}. This latter value is in better agreement with the value estimated by Mills[10] of -108 ± 10 kcal mol^{-1}, than the value reported by Tuenge from mass spectrometry data (-83 ± 5 kcal mol^{-1}). Tuenge's value for the cohesive energy could be improved by 6 kcal mol^{-1} if the slope of ln P_{Sc} vs T^{-1} were used instead of the activity of ScS evaluated at only one temperature. Furthermore, the value of the heat of formation obtained in this work for $Sc_{1.00}S(s)$ agrees well with the corresponding quantities for YS(s) (-109 kcal mol^{-1} [3]), for LaS(s) (-105 kcal mol^{-1} [11]) and for LuS(s) (-99.6 ± 3.1 kcal mol^{-1} [12]).

A comparison of the atomization or cohesive energy of these solids may provide revealing insight into the role of the d electron in the bonding character. Table 2.8 lists the atomization enthalpies for the stoichiometric monosulfides, ScS, YS, LaS and LuS. The constant value for YS and LaS suggests that the contribution of the d electron to the metal-metal and metal-nonmetal bonding interactions is similar, while the smaller enthalpies for ScS and LuS suggest a decrease in the d electron participation. This trend in the cohesive energies may be responsible for the observation that ScS and LuS vaporize incongruently at high

Table 2.8. Atomization enthalpies for ScS, YS, LaS and LuS

	$\Delta H^{\circ}_{atom,298\ K}$ (kcal mol^{-1})	Reference
ScS	255.7 ± 2.6	This work
YS	278 ± 2	3
LaS	275 ± 3	11
LuS	268.5 ± 3.0	12

temperature to form $Sc_{0.8065}S$ and Lu_3S_4, respectively, while YS and LaS vaporize congruently. Another contributing factor is the notion that the 4d and 5d wavefunctions extend to larger radial distances than the 3d wavefunction and therefore an enhancement in the metal-metal bonding interaction in YS and LaS compared to ScS.

REFERENCES CITED

1. Tuenge, R. T.; Laabs, F.; Franzen, H. F. J. Chem. Phys. 1976, 65, 2400.

2. Coppens, P.; Smoes, S.; Drowart, J. Trans. Faraday Soc. 1967, 63, 2140.

3. Steiger, R. P. Ph.D. Dissertation, University of Iowa, Iowa City, IA, 1967.

4. Moodenbaugh, A. R. Ph.D. Dissertation, University of California, San Diego, CA, 1975.

5. Kematick, R.; Anderegg, J.; Franzen, H., 4th International Conference on High Temperature and Energy-Related Materials, Santa Fe, NM, April 2-6, 1984, to be published in High Temp. Sci.

6. Knudsen, M. Ann. Physik 1909, 29, 179.

7. Tuenge, R. T. Ph.D. Dissertation, Iowa State University, Ames, IA, 1975.

8. Hultgren, R.; Desai, P. D.; Hawkins, D. T.; Gleiser, M.; Kelley, K. K.; Wagman, D. D. "Selected Values of the Thermodynamic Properties of the Elements", American Society for Metals: Metals Park, OH, 1973.

9. Stull, D. R., Ed. "JANAF Thermochemical Tables", 2nd ed. ; U. S. Government Printing Office: Washington, D.C., 1971; NSRDS-NBS 37.

10. Mills, K. C. "Thermodynamic Data for Inorganic Sulfides, Selenides and Tellurides", Butterworths and Co., Ltd.: London, 1974.

11. Cater, E. D.; Steiger, R. P. J. Phys. Chem. 1968, 72, 2231.

12. Franzen, H. F.; Hariharan, A. V. J. Chem. Phys. 1979, 70, 4907.

GENERAL SUMMARY

From the results of the self-consistent electronic structure calculations, metal atom vacancies (a) cause the p-type wavefunctions centered on a sulfur atom in the vicinity of a vacancy to redistribute and create nonbonding states and (b) increase the metal-nonmetal hybridization in the valence band region such that the scandium valency remains unchanged.

The charge density in the valence band region is altered when metal atom vacancies are created: the three-fold symmetry of the usual covalent σ-bonding interaction is destroyed. There is an appreciable reduction in the Sc e_g-octahedral S p interaction but an overwhelming compensation in the Sc e_g-square planar S p interaction. In both ScS and Sc_3S_4, the primary bonding interaction in the conduction band region originates from the projection of the metal t_{2g} orbitals out towards the triangular faces of the sulfur polyhedron. In addition, a secondary metal-metal interaction, observed from the charge density analysis, is directed towards the nearest neighbor metal atoms through the edges of the sulfur polyhedron.

The creation of vacancies was shown to lower the Fermi level suggesting an energetic mechanism for vacancy stabilization, but the details of the mechanism could not be determined from this work. The results for stoichiometric ScS are in good agreement with existing experimental results, including UPS, heat capacity and optical data, while experimental data are lacking for the nonstoichiometric material.

The thermodynamic quantities obtained from the mass loss Knudsen effusion experiments were (a) the temperature independent activity of ScS in $Sc_{0.8065}S(s)$, $a_{ScS} = 0.48 \pm 0.05$ over the temperature span of 1950-2100 K, (b) the energy required to create approximately 20% scandium vacancies in ScS, 25.0 ± 1.8 kcal mol^{-1} at 298 K, (c) the atomization or cohesive energy of ScS, 255.7 ± 2.6 kcal mol^{-1} at 298 K, and (d) the heat of formation of ScS, -98.7 ± 2.8 kcal mol^{-1} at 298 K. The value of the heat of formation is in good agreement with the value predicted by Mills[19] and the value reported for LuS,[20] which like ScS has the same effective metal electron configuration $[(n)d^1(n+1)s^2$, ignoring the filled f-shell for Lu], and vaporizes incongruently to form a more stable metal-deficient compound at high temperature.

FUTURE CONSIDERATIONS

Suggestions for future work include the calculation of the total energies (i.e., cohesive or lattice energies) for ScS and Sc_3S_4 to further understand the mechanism of vacancy formation and stabilization. Using the self-consistent crystal potential and wavefunctions, the total energy can be calculated from the theoretical formalism of Janak.[21] The difference between the calculated total energy of the compound and the sum of the isolated atom total energies, is related to the cohesive energy of the compound. In turn, the theoretically derived cohesive energy is related to the thermodynamically determined enthalpy of atomization at absolute zero.

A preliminary total energy result for NaCl-type ScS in which the sulfur 3s level is a band state and the core potential in the interstitial region is continuous, is -2311.447 Ry. Taking the sum of the isolated atom total energies to be -2310.734 Ry (S = -793.412 Ry[22] and Sc = -1517.322 Ry[23]), yields a cohesive energy equal to -0.713 Ry or an enthalpy of atomization equal to 224 kcal mol^{-1} which can be compared to the experimental value of this work, 256.6 ± 3.1 kcal mol^{-1}. Once the total energies of both ScS and Sc_3S_4 are known, their difference is an estimation of the energy required to create vacancies in the scandium sublattice. The result could then be compared to the experimental value of 25.1 ± 2.3 kcal mol^{-1}.

Another area which requires additional effort is the experimental confirmation of the electronic structure of nonstoichiometric scandium monosulfide. Suggestions are heat capacity measurements as a function of

composition to monitor the density of states at the Fermi level and X-ray emission and/or photoelectron experiments to provide evidence of the sulfur 3p-nonbonding states.

Finally, additional mass loss Knudsen effusion experiments are necessary in order to determine the extent of the metal solubility in $Sc_{1.00}S$ and to generate a plot of ln P_i vs T^{-1} as a function of composition. From this plot, thermal functions like the partial molar enthalpy and partial molar entropy of Sc and S can be determined.

ADDITIONAL REFERENCES CITED

1. Ashcroft, N. W.; Mermin, N. D. "Solid State Physics"; Holt, Rinehart and Winston: New York, 1976.

2. Franzen, H. F. Prog. Solid State Chem. 1978, 12, 1.

3. Watanabe, D.; Castles, J. R.; Jostsons, A.; Malin, A. S. Acta Cryst. 1967, 27, 307.

4. Bowman, A. L.; Wallace, T. C.; Yarnell, J. L.; Wenzel, R. G. Acta Cryst. 1966, 21, 843.

5. Holmberg, B. Acta Chem. Scand. 1962, 16, 1255.

6. Brauer, G.; Schnell, W.-D. J. Less-Common Metals 1964, 6, 326.

7. Conard, B. R.; Franzen, H. F. "The Chemistry of Extended Defects in Non-Metallic Solids"; L. Eyring and M. O'Keeffe, Eds.: North Holland: Amsterdam, 1970.

8. Dismukes, J. P.; White, J. G. Inorg. Chem. 1964, 3, 1220.

9. Tuenge, R. T. Ph.D. Dissertation, Iowa State University, Ames, IA, 1975.

10. Tuenge, R. T.; Laabs, F.; Franzen, H. F. J. Chem. Phys. 1976, 65, 2400.

11. Merrick, J. A. Ph.D. Dissertation, Iowa State University, Ames, IA, 1980.

12. Huisman, L. M.; Carlsson, A. E.; Gelatt, C. D., Jr.; Ehrenreich, H. Phys. Rev. B 1980, 22, 991.

13. Denker, S. P. J. Less-Common Metals 1968, 14, 1.

14. Goodenough, J. B. Phys. Rev. B 1972, 5, 2764.

15. Brozek, V.; Flahaut, J.; Guittard, M.; Julien-Pouzel, M.; Pardo, M.-P. Bull. Soc. Chim. Fr. 1974, 9/10, 1740.

16. Takeshita, T.; Beaudry, B. J.; Gschneidner, K. A., Jr., Ames Laboratory, private communication.

17. Franzen, H. F.; Tuenge, R. T.; Eyring, L. J. Solid State Chem. 1983, 49, 206.

18. Moodenbaugh, A. R.; Johnston, D. C.; Viswanathan, R. Mat. Res. Bull. 1974, 9, 1671.

19. Mills, K. C. "Thermodynamic Data for Inorganic Sulfides, Selenides and Tellurides", Butterworths and Co., Ltd.: London, 1974.

20. Franzen, H. F.; Hariharan, A. V. J. Chem. Phys. 1979, 70, 4907.

21. Janak, V. F. Phys. Rev. B 1974, 9, 3985.

22. Misemer, D. K., Ames Laboratory, private communication.

23. Moruzzi, V. L.; Janak, J. F.; Williams, A. R. "Calculated Electronic Properties of Metals"; Pergamon Press, Inc.: New York, 1978.

ACKNOWLEDGEMENTS

This dissertation would not exist without the support and encouragement of many people. I wish to thank Professor Hugo Franzen and Dr. David Misemer for their guidance, patience and their invaluable suggestions provided throughout this research project. Many thanks to Jim Anderegg for the maintenance of the mass loss-mass spec apparatus, rewriting data acquisition software and technical expertise. To the past and present group members, I thank you for your friendship and helpful discussions.

Special thanks to my parents and siblings who have waited so patiently and never gave up, and to my husband, Tommy, who was always willing to lend an open ear and boost my confidence.

Last but not least, I wish to thank my adopted mother, Shirley Standley, who has provided much assurance and encouragement and who spent many precious hours typing this dissertation.